NASA TN D-288

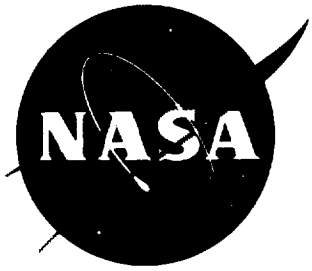

TECHNICAL NOTE

D-288

NASA RESEARCH ON THE HYDRODYNAMICS OF THE GASEOUS VORTEX REACTOR

By Robert G. Ragsdale

Lewis Research Center
Cleveland, Ohio

NATIONAL AERONAUTICS AND SPACE ADMINISTRATION
WASHINGTON

NATIONAL AERONAUTICS AND SPACE ADMINISTRATION

TECHNICAL NOTE D-288

NASA RESEARCH ON THE HYDRODYNAMICS OF THE GASEOUS VORTEX REACTOR*

By Robert G. Ragsdale

SUMMARY

The experimental and analytical results to date of a study of a two-component gaseous vortex system are presented in this paper. Analytical expressions for tangential velocity and static-pressure profiles in a turbulent vortex show good agreement with experimental data. Airflow rates from 0.075 to 0.14 pound per second and corresponding tangential velocities from 160 to 440 feet per second are correlated by turbulent Reynolds numbers from 1.95 to 2.4.

An analysis of an air-bromine gas mixture in a turbulent vortex indicates that a boundary value of bromine-to-air radial velocity ratio $(u_2/u_1)_o$ of 0.999 gives essentially no bromine buildup, while a value of 0.833 results in considerable separation. For a constant value of $(u_2/u_1)_o$, the bromine buildup increases as (1) the tangential velocity increases, (2) the air-to-bromine weight-flow ratio decreases, (3) the airflow rate decreases, (4) the temperature decreases, and (5) the turbulence decreases. Analytical temperature, pressure, and tangential-velocity profiles are also presented.

Preliminary experimental results indicate that the flow of an air-bromine mixture through a vortex field results in a bromine density increase to a maximum value, followed by a decrease; the air density exhibits a uniform decrease from the outer vortex radius to the exhaust-nozzle radius.

INTRODUCTION

The concept of a gaseous nuclear reactor is relatively new but is extremely attractive for use as a space-propulsion device. Solid-fuel-element reactors are limited in performance by temperature restrictions placed by the heat-transfer surface. Proposed liquid-fuel reactors are limited by evaporation losses occurring near the boiling point of the fissionable liquid. The containing walls of a cavity reactor are obviously still subject to the same materials limiting temperature, but this

*This paper was presented before a closed session of the annual meeting of the American Rocket Society, Washington, D.C., Nov. 16-21, 1959. By agreement with the American Rocket Society, the NASA is publishing this material.

is not the temperature at which energy is transferred to the propellant gas. An intimate mixture of a fissionable gas and a propellant gas is introduced at the outer perimeter, cools the wall surfaces, and flows toward the center of the cavity where, as critical conditions are attained, the fission energy is imparted directly to the propellant. Figure 1 illustrates this flow pattern. Some considerations of gaseous or "cavity" reactors are given in references 1 to 3.

Although potential operating temperatures of the order of 2×10^4 $^{\circ}$ R and specific impulses greater than 1800 seconds offer mission capabilities not possible with "conventional" heat-transfer rockets, the cost incurred by the ejection of the fissioning gas (UF_6, e.g.) at its critical concentration is prohibitive (refs. 4 to 7). A practical gaseous-reactor propulsion device must therefore eject only a small fraction, say 1/1000 or less, or the critical mass of fission gas per throughput of propellant gas. This means that essentially all the uranium gas must be retained in the cavity by some force field through which the propellant gas, hydrogen, can flow.

One such force currently considered (refs. 4 to 7) is that generated by vortex-type flow of the hydrogen-uranium mixture through the cavity. The fundamental mechanism utilized is that of inertia; the rapid acceleration of the gas mixture is resisted by each of the gases and, because of the difference in mass, to a different degree. The result is that the heavy gas accelerates less than the light one and thus has a longer holdup time in the vortex chamber. The resulting buildup of heavy molecules then presents what is essentially a fissioning barrier through which the light molecules must diffuse. Figure 2 illustrates such a device.

There are of course many problems to be resolved in order to predict the performance of this system. These problems (the heat-transfer mechanism, critical studies, hydrodynamic performance, etc.) when considered together make an analysis tremendously complex. Extensive analyses of such a vortex system have been published (refs. 4 and 5). Certain assumptions as to idealized conditions were necessary to permit resolution of the equations involved.

The hydrodynamic study presented in this paper represents the result of an alternative approach, a stepwise consideration of the total problem. An attempt was made to interpret, analytically and experimentally, the degree of turbulence present in a real vortex generator and the associated effect on pressure, temperature, and velocity profiles. The results of similar studies are given in references 8 to 11. Next, using this turbulence information, an analysis was made of a light gas diffusing through a heavy one in a turbulent vortex field at room temperature. The analysis was then applied to a system of real gases, air and bromine, and an experimental program was undertaken to verify the analytical

results. The purpose of the experiment was twofold: The first phase was to determine the degree of turbulence present in the vortex for various flow conditions; the second phase was to measure variations in bromine density at various radii.

SYMBOLS

B_2	bromine density, molecules/(cc)(lb sq in. abs)
B_2^*	bromine density normalized to vortex header
b	dimensionless parameter defined in eq. (20)
C	constant of integration in eq. (15)
c	concentration, atoms/cc
c_p	specific heat at constant pressure, Btu/(lb)(^oF)
D_{12}	laminar binary diffusion coefficient, sq ft/sec
g	gravitational constant, ft/sec^2
I	transmitted light intensity, lumens
I_0	initial light intensity, lumens
J	mechanical equivalent of heat, ft-lb/Btu
k	thermal conductivity, Btu/(sq ft)(sec)(^oF/ft)
L	vortex chamber length, ft or in.
l	path length, cm
M	molecular weight, lb/lb-mole
m	specific extinction coefficient, cm^2/atom
n	molecular density, ρ/M, lb-mole/cu ft
P	total pressure, lb/sq ft
p	static pressure, lb/sq ft
R	universal gas constant, ft-lb/(lb-mole)(^oR)

E-800

CJ-1 back

Re	Reynolds number
r	radial coordinate, ft
T	total temperature, ^{o}R
t	static temperature, ^{o}R
u	radial velocity, ft/sec
V	molecular volume, cc/g-mole
v	tangential velocity, ft/sec
w	weight-flow rate, lb/sec
x	dimensionless radius, r/r_o
y	mole fraction
z	axial coordinate, ft
α_2	dimensionless parameter defined in eq. (20)
β	parameter defined in eq. (20), sq ft
γ	ratio of specific heats
ϵ	eddy diffusivity, sq ft/sec
θ	angular coordinate, radians
μ	viscosity, lb/(ft)(sec)
ρ	density, lb/cu ft
Φ	dissipation function, lb/(sq ft)(sec)
Ψ_1,Ψ_2,Ψ_3	algebraic functions

Subscripts:

n	exhaust nozzle
o	outer radius
l	light gas (air)

2 heavy gas (bromine)

Superscript:

' normalized to value at r_n

ANALYSIS

Assumptions

Throughout the analysis certain assumptions are made; some are implied and some are explicit. They are all set down here, but not necessarily in order of appearance or importance:

(1) Adiabatic flow ($k = 0$)

(2) $\partial/\partial\theta = \partial/\partial z = 0$

(3) Steady state

(4) Perfect gases

(5) No thermal diffusion or external forces considered in diffusion process

(6) Radial velocities and gradients small compared with tangential ones

(7) μ and $\rho\epsilon$ constant

(8) Laminar diffusion coefficient D_{12} given by the Gilliland relation (ref. 12):

$$D_{12} = 0.00404 \frac{t^{3/2}}{p\left(V_1^{1/3} + V_2^{1/3}\right)^2}\sqrt{\frac{1}{M_1} + \frac{1}{M_2}}$$

(9) Turbulent flow may be represented by laminar relations if μ is replaced by $\rho\epsilon$ and D_{12} is replaced by ϵ in concentration gradient term of diffusion equation.

Basic Equations

The general nomenclature for the analysis is as indicated in the following sketch:

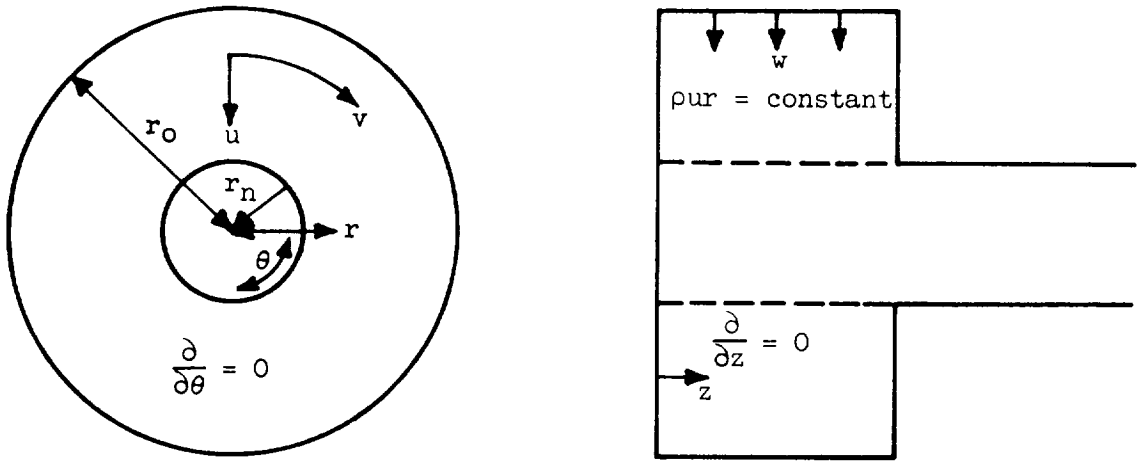

Vortex analytical model

The equations requiring that the system conserve fluid momentum are the Navier-Stokes relations (ref. 13). For compressible flow and $\partial/\partial\theta = \partial/\partial z = 0$, they may be written

$$\rho u \frac{\partial u}{\partial r} - \rho \frac{v^2}{r} = - \frac{\partial p}{\partial r} + \frac{\partial}{\partial r}\left\{\mu\left[2 \frac{\partial u}{\partial r} - \frac{2}{3r} \frac{\partial (ru)}{\partial r}\right]\right\} + \frac{2\mu}{r}\left(\frac{\partial u}{\partial r} - \frac{u}{r}\right) \tag{1}$$

$$\rho u \frac{\partial v}{\partial r} + \rho u \frac{v}{r} = \frac{\partial}{\partial r}\left[\mu\left(\frac{\partial v}{\partial r} - \frac{v}{r}\right)\right] + \frac{2\mu}{r}\left(\frac{\partial v}{\partial r} - \frac{v}{r}\right) \tag{2}$$

The conservation of system energy for adiabatic flow (k = 0) is expressed as (ref. 13)

$$(\rho u c_p) \frac{\partial t}{\partial r} - u \frac{\partial p}{\partial r} = \Phi = \mu\left[2\left(\frac{\partial u}{\partial r}\right)^2 + 2\left(\frac{u}{r}\right)^2 + \left(\frac{\partial v}{\partial r} - \frac{v}{r}\right)^2 - \frac{2}{3}\left(\frac{\partial u}{\partial r} - \frac{u}{r}\right)^2\right] \tag{3}$$

The continuity equation for steady-state flow becomes

$$\frac{\partial (\rho u r)}{\partial r} = 0 \tag{4}$$

The assumption of a perfect gas gives

$$p = \frac{\rho R t}{M} \tag{5}$$

as the equation of state.

The diffusional transport relation, neglecting thermal diffusion and external forces, is written as (ref. 14)

$$(u_1 - u_2) = \frac{-n^2}{n_1 n_2} D_{12}\left[\frac{\partial(n_1/n)}{\partial r} + \frac{n_1 n_2 (M_2 - M_1)}{n\rho} \cdot \frac{1}{p}\frac{\partial p}{\partial r}\right] \tag{6}$$

These are the basic equations forming the nucleus of the analysis. Certain assumptions were made as they were written down. Additional assumptions are required to transform them into useful working equations.

Ideal Fluid Motion (Inviscid Flow)

With the assumptions that $\mu = 0$ and that radial velocity functions are small compared with corresponding tangential ones, the following familiar relations are obtained from equations (1) to (5):

$$P = p\left(1 + \frac{\gamma - 1}{2}\frac{Mv^2}{\gamma g R T}\right)^{\frac{\gamma}{\gamma-1}} = \text{Constant} \tag{7}$$

$$T = t(P/p)^{\frac{\gamma-1}{\gamma}} = \text{Constant} \tag{8}$$

$$v = \frac{v_o r_o}{r} \tag{9}$$

$$w = u(2\pi r L)\rho \tag{10}$$

These equations, and all others presented herein, apply only to the annular region of the vortex. Equations (7) to (10), though useful as simple approximations, become less and less valid as higher vortex strengths are considered and are useful only for comparing real condition with ideal ones.

Real Fluid Motion (Laminar and Turbulent)

For real fluid motion it is convenient to define a Reynolds number as

$$Re \equiv -\frac{\rho u r}{\mu} \tag{11}$$

In reference 8, the continuity relation for the center core region $(0 < r < r_n)$ is assumed to be

$$\rho u r = (\rho_n u_n r_n)\left(\frac{r}{r_n}\right)^2 \tag{12}$$

and $v(0) = 0$, $v(r_n) = v_n$ are taken as boundary conditions. Equation (2) then yields the tangential-velocity profile:

$$v' = \frac{1}{r'}\,\frac{1 - e^{-\frac{Re(r')^2}{2}}}{1 - e^{-Re/2}} \tag{13}$$

For the annular region $(r_n < r < r_o)$, using equation (4) and the boundary condition $v(r_o) = v_o$ with equation (2) gives the velocity profile in the form

$$v' = \frac{v_o' r_o'}{r'}\sqrt{\Psi_1} \tag{14}$$

where

$$\Psi_1 = \left(\frac{1}{v_o' r_o'}\right)^2\left[(1 - C)^2 + 2\,\frac{C - C^2}{(r')^{Re-2}} + \frac{C^2}{(r')^{2Re-4}}\right]$$

In equations (13) and (14) and all succeeding ones, the prime refers to the quantity normalized to its value at the radius r_n; this is, analytically, the smallest radius at which equation (4) applies, and, numerically, is taken to be the exhaust-nozzle radius.

The constant C in the Ψ_1 function remains to be evaluated by some boundary condition. A continuous velocity profile is obtained by equating the velocity derivatives from equations (13) and (14). This gives

$$C = \left(\frac{1}{2 - Re}\right)\frac{Re}{e^{Re/2} - 1} \tag{15}$$

It is of interest to note that a different boundary condition, $(dv'/dr')_{r'=1} = 0$, yields

$$C = \frac{1}{2 - Re}$$

Equation (15) is used throughout this paper, and if substituted into equation (14) gives the same result as was obtained in reference 8. As $Re \to \infty$ (inviscid flow), $\psi_1 \to 1$, and equation (14) yields equation (9). This suggests that the function ψ_1 may be viewed as a "correction factor" to account for viscous effects on the ideal velocity profile.

Equations (1), (3), (4), and (5) may be combined, and the boundary condition $t(\infty) = T_\infty$ applied to give the energy relation

$$T_\infty = t + \frac{\frac{1}{2}\left(\frac{v_o r_o}{r}\right)^2 (\psi_2 - \psi_3)}{c_p g J} \tag{16}$$

where

$$\psi_2 = \left(\frac{1}{v_o' r_o'}\right)^2 \left[(1 - C)^2 + \left(\frac{4}{Re}\right)\frac{C - C^2}{(r')^{Re-2}} + \frac{C^2}{Re - 1}\frac{1}{(r')^{2Re-4}}\right]$$

$$\psi_3 = \left(\frac{1}{v_o' r_o'}\right)^2 \left[\frac{4}{Re}(1 - C)^2 + \left(\frac{8}{Re}\right)\frac{C - C^2}{(r')^{Re-2}} + \frac{ReC^2}{Re - 1}\frac{1}{(r')^{2Re-4}}\right]$$

The function ψ_2 represents the effect of viscosity on radial momentum, and ψ_3 the effect of the viscous dissipation term, the right side of equation (3). As before, when $Re \to \infty$, $\psi_2 \to 1$, $\psi_3 \to 0$, and equation (16) gives the isentropic relation. Equation (16) gives the variation of static temperature with radius. The total-temperature variation is given by

$$T = t + \frac{v^2}{2c_p g J} \tag{17}$$

where v is given as a function of radius by equation (14).

The continuity equation (4) in integrated form is

$$\frac{w}{2\pi L r} = \rho u = \rho_1 u_1 + \rho_2 u_2 = \frac{w_1 + w_2}{2\pi L r} \tag{18}$$

Equations (1) and (6) are nonlinear and are solved simultaneously by the Runge-Kutta numerical method. Combining these equations with equations (5) and (18) gives the working equations as

$$\frac{1}{p/p_o}\frac{d(p/p_o)}{dx} = \frac{(y_1M_1 + y_2M_2)v^2}{gRt} \tag{19}$$

$$\frac{dy_2}{dx} = \frac{-\alpha_2(by_2 - 1)}{x} + \frac{\beta(y_2 - y_2^2)}{x^3} \tag{20}$$

where

$$\alpha_2 = \frac{w_2}{2\pi LD_{12}n} \qquad b = 1 + \frac{w_1}{w_2}\frac{M_2}{M_1} = \frac{1}{y_{2,\infty}}$$

$$\beta = \frac{(M_2 - M_1)v_o^2\psi_1}{gRt} \qquad y_{2,o} = \frac{1}{1 + \left(\frac{w_1}{w_2}\right)\left(\frac{M_2}{M_1}\right)\left(\frac{u_2}{u_1}\right)_o}$$

The boundary condition for equation (19) is $(p/p_o)_{x=1} = 1$, and for (20) is $(u_2/u_1)_{x=1} = (u_2/u_1)_o$. The subscripts 1 and 2 refer to the light and heavy gases, respectively. The laminar diffusion coefficient D_{12} is calculated from the Gilliland relation:

$$D_{12}n = \frac{2.62\times10^{-6}\sqrt{t}\left(\frac{1}{M_1} + \frac{1}{M_2}\right)^{1/2}}{\left(V_1^{1/3} + V_2^{1/3}\right)^2} \tag{21}$$

The total-pressure relation is

$$P = p\left[1 + \frac{\gamma - 1}{2}\frac{(y_1M_1 + y_2M_2)v^2}{\gamma gRt}\right]^{\frac{\gamma}{\gamma-1}} \tag{22}$$

All the working equations necessary to define the system (eqs. (14) to (22)) as written are for laminar flow. That is, Re is given by equation (11). These equations were converted to turbulent flow by the assumption

$$Re_{turbulent} = Re_{laminar} \cdot \frac{\mu}{\mu + \rho\epsilon} \simeq Re_{laminar} \cdot \frac{\mu}{\rho\epsilon}$$

With the exception of equation (20), all equations remain as given, and the Reynolds number is now

$$Re \equiv \frac{-u_o r_o}{\epsilon} = \frac{w}{2\pi L\rho_o\epsilon} \tag{23}$$

Reference 8 gives an approximate expression for ϵ as a function of tangential velocities and gradients. Since there exists little or no experimental verification of this expression, the Re values reported herein were obtained by a curve-fitting (pressure and velocity) procedure described in the section RESULTS AND DISCUSSION. To rewrite the diffusion equation (6) for turbulent flow, it was assumed that the turbulent eddies affect the concentration-gradient term, $(\partial/\partial r)(n_1/n)$, but that the pressure-gradient term is unaffected by eddy mixing. This results in the multiplication of the right side of equation (20) by the ratio $D_{12}n/\epsilon n$, where

$$\epsilon n = \left[\frac{w}{2\pi LRe(y_{1,o}M_1 + y_{2,o}M_2)}\right]\left(\frac{p}{p_o}\right)\left(\frac{t_o}{t}\right) \tag{24}$$

These are the equations as used. The one input value required but unavailable is $(u_2/u_1)_o$. The analysis is written for an unbounded flow field, but applied to a bounded volume, namely a real vortex of radius r_o. Were the vortex of infinite radius, the value of $(u_2/u_1)_o$ would be 1. For no radial bromine flow, $(u_2/u_1)_o$ becomes 0. Therefore, values of $(u_2/u_1)_o$ between 0 and 1 should be expected, and values near 1 would seem intuitively to be realistic. Lacking analytical equations describing the fluid-wall boundary conditions, numerical values were assigned to $(u_2/u_1)_o$, and families of curves were obtained with $(u_2/u_1)_o$ as the parameter.

EXPERIMENT

The vortex test apparatus was designed to provide (1) high tangential velocities (~500 ft/sec) and low mass flows (~0.1 lb/sec), (2) measurements of total and static pressures, (3) the introduction of homogenous air-bromine gas mixtures, and (4) measurements of radial bromine concentrations in an undisturbed vortex field. Figure 3 illustrates the vortex test section and gives dimensions. The test section was fabricated of Lucite to permit visual observation. Glass windows were inserted to provide a transparent path for the optical instrumentation (fig. 4). The blades forming the cylindrical perimeter were made of Inconel. Static-pressure taps were located radially, and total-pressure probes (0.030-in. O.D., 0.003-in. wall) were inserted as shown in figure 4. Air weight flows were measured with an upstream orifice run. Figure 5 shows a schematic diagram of the overall test setup. The dry air was regulated to maintain atmospheric pressure in the vortex header and exhausted to an altitude exhaust system (26-in.-Hg vacuum, max.). Bromine gas was generated by means of a 500-watt boiler and a variable voltage control and was introduced into the airstream ahead of the test section. Figure 6 is a photograph of the entire system.

Optical measurements were made by passing light beams through the test section at various radii. The outputs of photomultipliers were recorded on a multichannel oscillograph. The absorption spectra of bromine gas and light filters were matched to provide maximum sensitivity to the presence of bromine (fig. 7). The locations of the multireflected, single light source and the photomultipliers are shown in figure 8. Figure 9 shows the instrumentation equipment in relation to the vortex generator. The photomultipliers were calibrated with light filters of measured optical density at the wavelength used in the experiment. The nonlinearity shown in figure 10 is a characteristic of the oscillograph used and not of the photomultipliers. Calibration curves from measured voltage ratios rather than oscillograph-trace ratios were linear for every photomultiplier.

To determine the turbulence effects, static- and total-pressure measurements were made. These and total-temperature measurements have been previously reported (ref. 9). Though certain variations in inlet nozzle design were attempted, an appreciable energy loss, reflected in a drop in total pressure, was found to limit the vortex tangential velocities, measured at radius of 4.75 inches, to around 500 feet per second. This entrance loss phenomenon is also reported in reference 10, and a possible method of its reduction is suggested in reference 15.

RESULTS AND DISCUSSION

Turbulence

With air as the fluid, a series of experimental runs was made to determine the deviation of real vortex flow from ideal conditions. Static and total pressures were measured at various radii for weight flows ranging from 0.075 to 0.14 pound per second. The pressure in the vortex header was maintained at or near atmospheric pressure, and the exhaust pressure was varied from near 1 to 26 inches of mercury. Equations (16) and (22), with $y_1 = 1$ and $y_2 = 0$, were used to calculate experimental tangential velocities.

Velocity data for a typical run are shown in figure 11. The data points were originally plotted as absolute values, and equation (14) was used to determine the necessary v_o and Re within 2 percent to fit the curve to the data. The two data points were then normalized to r_o by dividing by this value of v_o. For comparison, the curve representing inviscid flow (Re = ∞) is shown. The tangential velocity is seen to increase from r_o to r_n, but not as rapidly as that of an ideal fluid.

The value of Re determined from the velocity data was then used with equations (14), (16), and (19) to calculate an analytical static-pressure curve. Figure 12 (for the same run as fig. 11) shows this curve, the one for ideal flow, and the actual static-pressure data. The fit of the curve to the data, while not perfect, is seen to be a much better approximation than inviscid flow.

The procedure indicated in figures 11 and 12 provides a means of experimentally determining a turbulent Reynolds number from static- and total-pressure data. For weight flows of 0.075 to 0.14 pound per second, and corresponding v_o values of 160 to 440 feet per second, turbulent Reynolds numbers were found to vary from 1.95 to 2.4.

Two-Component Separation

Analytical. - Equations (14) to (19), (20), modified by $(D_{12}n/\epsilon n)$, (21), (22), and (24) were programmed on an IBM 704 computer to be solved by the Runge-Kutta numerical method. Input values of $(u_2/u_1)_o$, v_o, w_1/w_2, w_1, T_∞, and Re were assigned, and radial bromine densities and temperature, pressure, and velocity profiles were computed. The mole fraction y_2 in equation (20) is related to the actual bromine density by the simple relation

$$B_2 \equiv \frac{1.385 \times 10^{24}}{Rt}\left(\frac{p}{p_o}\right)y_2 \qquad \frac{\text{molecules}}{(\text{cc})(\text{lb/sq in.})}$$

All results are shown in terms of bromine density normalized to the outer radius, x = 1.

The effect of $(u_2/u_1)_o$, probably the most important and certainly the most elusive of the parameters affecting separation, on the radial bromine density variation is shown in figure 13(a). The effect of $(u_2/u_1)_o$ is readily apparent; a value of 0.999 gives essentially no separation, while one of 0.833 causes considerable buildup, the peak or maximum value occurring within the exhaust-nozzle radius. The importance of an understanding of the factors affecting this parameter is emphasized by the results shown in figure 13(a).

The remaining analytical density curves are for a $(u_2/u_1)_o$ value arbitrarily selected as 0.916. Conclusions as to the effect of the parameters shown in figures 13(b) to (f) must be drawn with caution; there is no assurance that $(u_2/u_1)_o$ is not a function of one or more of these parameters. For example, figure 13(b) suggests that an increase

in tangential velocity results in an increased separation, if $(u_2/u_1)_o$ does not increase sufficiently with the velocity increase to override its effect. Information as to the interdependence of the various parameters shown must ultimately come from experimental data.

Figures 13(b) to (f) show the effect of the various parameters on separation for $(u_2/u_1)_o = 0.916$. The indicated effects are obvious and, for the reason just discussed, do not justify extensive discussion or conclusions. The trends shown are summarized here. For constant $(u_2/u_1)_o$:

(1) Bromine buildup increases as v_o increases.

(2) Bromine buildup increases (slightly) as w_1/w_2 decreases.

(3) Bromine buildup increases (slightly) as w_1 decreases.

(4) Bromine buildup increases as T_∞ decreases.

(5) Bromine buildup increases as Re increases.

(6) Bromine buildup increases as turbulence decreases.

Analytical temperature profiles were computed and are shown in figure 14. The general trend indicated by the total-temperature curve is in agreement with the data reported in reference 9 and the analytical curves presented and discussed in reference 8. Briefly, the indicated rise in total temperature to a maximum value is a result of the shear work done by the fluid in itself as a result of tangential gradients.

Figure 15 shows the variation of static- and total-pressure ratios with radius. Again, these curves are in general agreement with the data of reference 9 and the analytical results in reference 8.

Figure 16 shows tangential- and radial-velocity variations. The tangential-velocity curve simply reflects the combined effects of the static- and total-pressure variations shown in figure 15. The air radial velocity is shown to increase uniformly with decreasing radius, while the bromine radial velocity increases to a maximum value and then decreases.

Experimental. - The experimental setup is designed to introduce uniform mixtures of air and bromine gas into a confined vortex field and to permit measurement of bromine density at various radii. Figure 5 shows this system. The 500-watt bromine boiler gives bromine flow rates from 0 to 0.006 pound per second; values of w_1/w_2 from 15 to 1500 are possible.

Light-intensity measurements are used to calculate the bromine concentrations; the optical instrumentation is shown in figures 8 and 9. Light beams are generated by multiple reflecting and focusing of a single light source, powered by a 6-volt storage battery. The light beams pass through filters, whose transmission characteristics are shown in figure 7, and are intercepted by photomultiplier tubes. The outputs of these tubes are recorded on a multichannel writing oscillograph. Typical photomultiplier calibration on curves, obtained with filters of measured optical densities, are shown in figure 10.

The data were reduced by the use of Beer's law of radiation. Reference 16 gives a comprehensive discussion of this law.

In equation form, Beer's law is

$$I/I_0 = e^{-mcl}$$

where m is the extinction coefficient, l is the path length through the absorbing medium, c is the concentration, and I_0 and I are the initial and transmitted light intensities, respectively. Writing this equation for two paths through the same medium, converting to logarithms, and dividing give

$$\frac{c_i}{c_H} = \frac{\ln(I/I_0)_i}{\ln(I/I_0)_H}$$

The subscript i represents any radius in the test section, and the subscript H refers to the vortex header, used as the reference point. The ratio c_i/c_H, called B_2^* herein, represents the ratio of bromine density at vortex radius r_i to the density in the header.

Figure 17 shows the results of a preliminary experimental run. These results are similar to those obtained from a series of runs. Some other typical results for various experimental conditions are shown in figure 18. The dashed line represents the air density variation calculated from equation (19). The data shown in figures 17 and 18 are preliminary, and no correlations or interpretations are given. It can be readily seen that there is apparently a measurable degree of separation. Were there no separation effect, the bromine density data would lie on the dashed line. The only statement justified from the data shown is that the flow of an air-bromine mixture through the vortex field results in a bromine density variation with radius that is measurably different from the air density change. A tentative corollary to this is that this bromine density deviation is in the direction desired to establish the feasibility of cavity reactor operation.

It is apparent from figures 13, 17, and 18 that the experimental and analytical separation results are not in agreement, even as to characteristic trends. The experimental data exhibit a maximum concentration nearer the outer wall than the exhaust nozzle. The analysis yields concentration increases near the exhaust nozzle. There are a number of possible explanations, some of which are: (1) Assumption (9) (ANALYSIS) is an oversimplification; (2) mixing lengths for mass and for momentum transfer are not the same; (3) laminar and eddy diffusion are not the only phenomena present. It is beyond the scope of this report to reevaluate the results with respect to these and other possible modifications. Fortunately, the experimental results indicate a greater degree of separation than the analysis predicts.

E-800

SUMMARY OF RESULTS

The research study, both analytical and experimental, on the hydrodynamics of a two-component gaseous vortex has been divided into a stepwise program. The results of a turbulence study undertaken to determine the degree of deviation of real vortex flow from ideal flow have been reported. An analysis of a mixture of air and bromine in turbulent vortex flow was given, and analytical curves were shown. Preliminary optical measurements of radial bromine density variations were presented. The following results were obtained:

1. Experimentally determined tangential-velocity profiles and static-pressure profiles are correlated by analytical equations containing a turbulent Reynolds number. For airflows from 0.075 to 0.14 pound per second and corresponding tangential velocities from 160 to 440 feet per second, turbulent Reynolds numbers from 1.95 to 2.4 were found to correlate the data.

2. The results of an analysis of an air and bromine mixture in a turbulent vortex indicate that:

(a) As the boundary value of the bromine-to-air radial-velocity ratio decreases, the degree of bromine buildup increases. For $(u_2/u_1)_o = 0.999$, there is no buildup; for $(u_2/u_1)_o = 0.833$, there is considerable buildup, the maximum point existing within the vortex exhaust-nozzle core. This parameter is the most important, but least understood, of those affecting the separation process. The indicated effects of the remaining parameters are valid only if $(u_2/u_1)_o$ is unaffected by their variation.

(b) Bromine buildup increases as tangential velocity v_o increases.

(c) Bromine buildup increases (slightly) as weight-flow ratio w_1/w_2 decreases.

(d) Bromine buildup increases (slightly) as air weight flow w_1 decreases.

(e) Bromine buildup increases as total temperature T_∞ decreases.

(f) Bromine buildup increases as Reynolds number Re increases.

(g) Bromine buildup increases as turbulence decreases.

3. Analytical radial variations of static and total temperature, static and total pressure, and tangential velocity for a turbulent vortex vary substantially from inviscid results and are in general agreement with published results of similar studies.

4. Experimentally determined radial bromine density variations are measurably different from the radial air density change. The bromine variation exhibits a buildup to a maximum at an intermediate radial position. This deviation from uniform flow is in the direction necessary to indicate the feasibility of cavity reactor operation.

Lewis Research Center
National Aeronautics and Space Administration
Cleveland, Ohio, March 10, 1960

REFERENCES

1. Shepherd, L. R., and Cleaver, A. V.: The Atomic Rocket-3. Jour. British Interplanetary Soc., vol. 8, no. 1, Jan. 1949, pp. 23-37.

2. Fox, R. H.: A Study of the Nuclear Gaseous Reactor Rocket. UCRL 4996, Lawrence Radiation Lab., Univ. Calif., Oct. 31, 1957.

3. Safanov, G.: Externally Moderated Reactors. Vol. 12 - Reactor Physics. Paper 625, Proc. Second United Nations Int. Conf. on Peaceful Uses of Atomic Energy (Geneva), 1958, pp. 705-718.

4. Grey, J.: A Gaseous-Core Nuclear Rocket Utilizing Hydrodynamic Containment of Fissionable Materials. Preprint 848-59, ARS, 1959.

5. Kerrebrock, J. L., and Meghreblian, R. V.: An Analysis of Vortex Tubes for Combined Gas-Phase Fission Heating and Separation of the Fissionable Material. CF-57-11-3, ORNL, Apr. 11, 1958.

6. Rom, Frank E.: Advanced Reactor Concepts for Nuclear Rocket Propulsion. Astronautics, vol. 4, no. 10, Oct. 1959, pp. 20-22, 46-50.

7. Bussard, Robert W.: Concepts for Future Nuclear Rocket Propulsion. Jet Prop., vol. 28, no. 4, Apr. 1958, pp. 223-227.

8. Deissler, R. G., and Perlmutter, M.: Analysis of the Flow and Energy Separation in a Turbulent Vortex. (To be publ. in Int. Jour. Heat and Mass Transfer.)

9. Savino, J. M., and Ragsdale, R. G.: Some Temperature and Pressure Measurements in Confined Vortex Fields. Preprint 60-SA-4, ASME, 1960.

10. Kerrebrock, J. L., and Keyes, J. J.: A Preliminary Experimental Study of Vortex Tubes for Gas-Phase Fission Heating. ORNL 2660, Feb. 20, 1959.

11. Mack, L. M.: The Compressible, Viscous, Heat-Conducting Vortex. Prog. Rep. 20-382, Jet Prop. Lab., C.I.T., May 1, 1959.

12. Perry, John H., ed.: Chemical Engineers' Handbook. Third ed., McGraw-Hill Book Co., Inc., 1950, p. 538.

13. Pai, Shih-I: Viscous Flow Theory. I - Laminar Flow. Ch. 3, D. Van Nostrand Co., Inc., 1956.

14. Chapman, Sydney, and Cowling, T. G.: The Mathematical Theory of Non-Uniform Gases. Cambridge Univ. Press, 1939, pp. 140-144.

15. Kerrebrock, J. L., and Lafayatis, R. G.: Analytical Study of Some Aspects of Vortex Tubes for Gas-Phase Fission Heating. CF-58-7-4, ORNL, July 21, 1958.

16. Lothian, G. F.: Absorption Spectrophotometry. Ch. 3, The Macmillan Co., 1958.

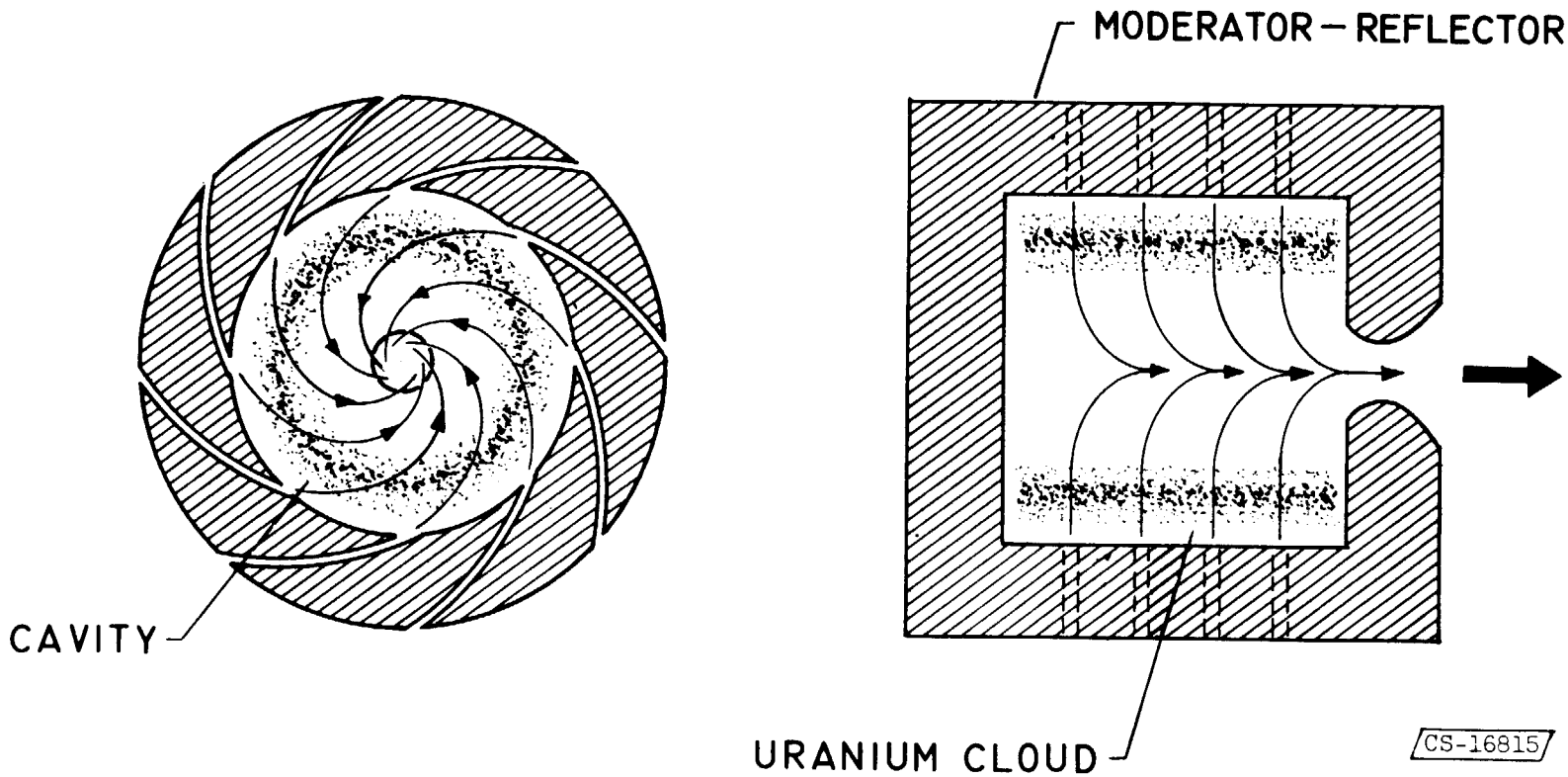

Figure 1. - Gaseous cavity reactor.

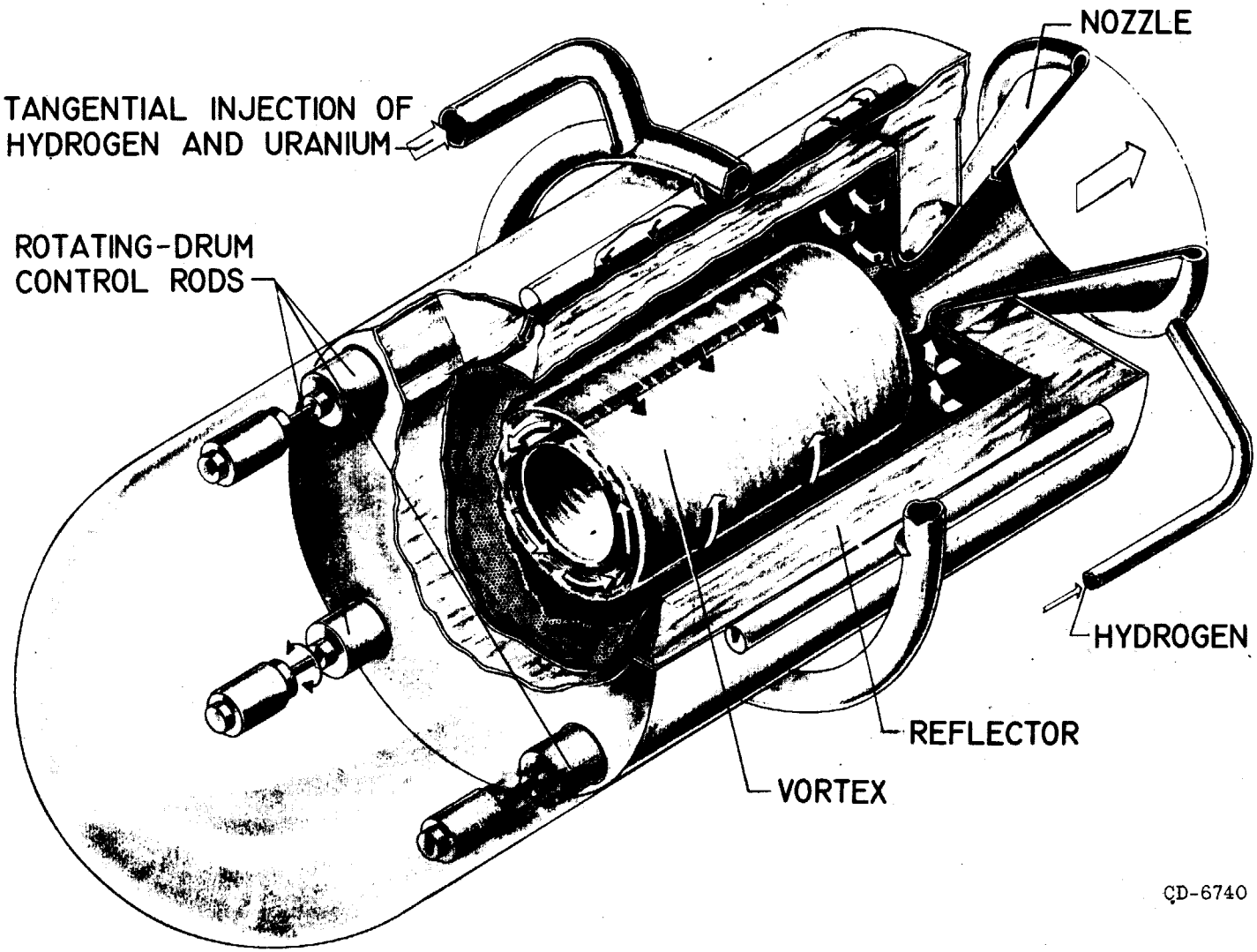

Figure 2. - Gaseous vortex reactor (from ref. 6).

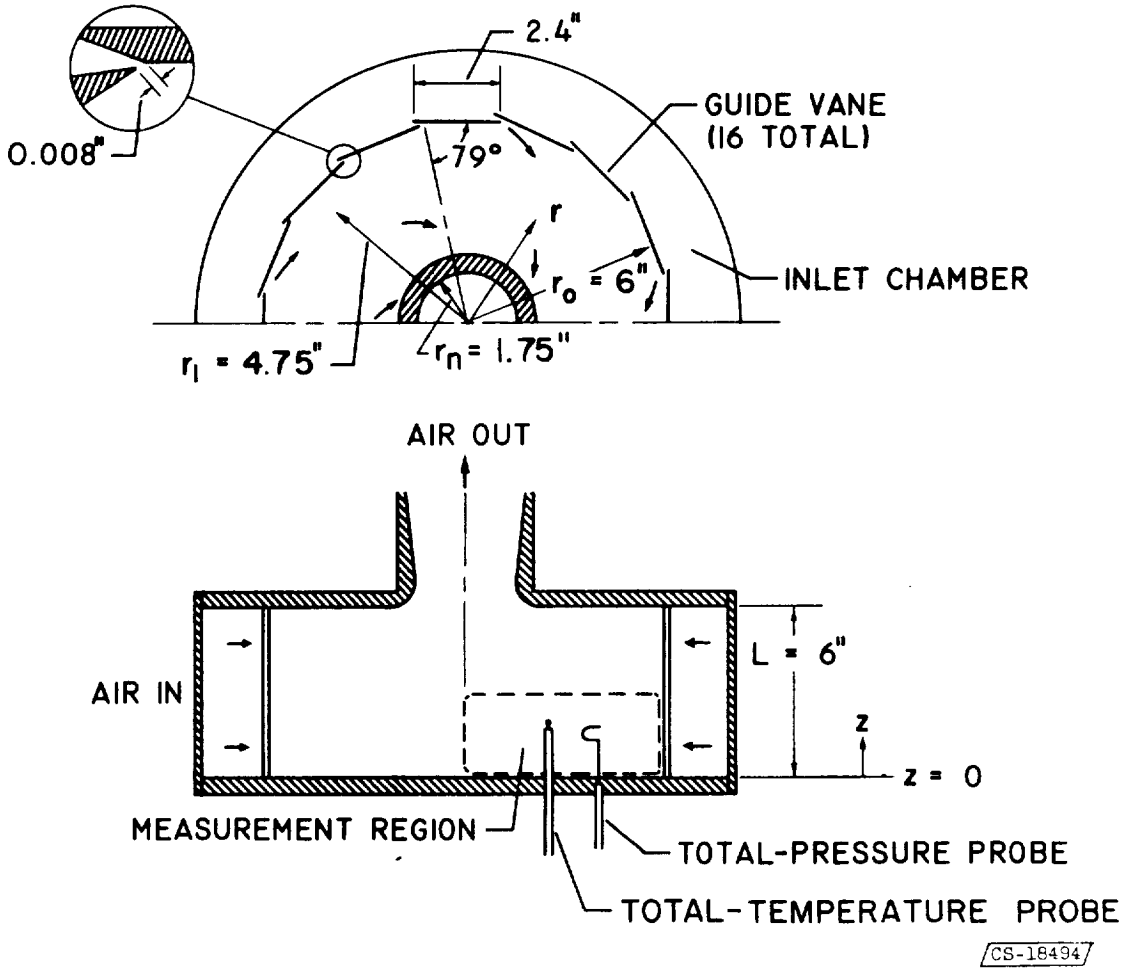

Figure 3. - Schematic drawing of vortex test section showing temperature- and pressure-measurement region.

CS-18477

Figure 4. - Vortex test section.

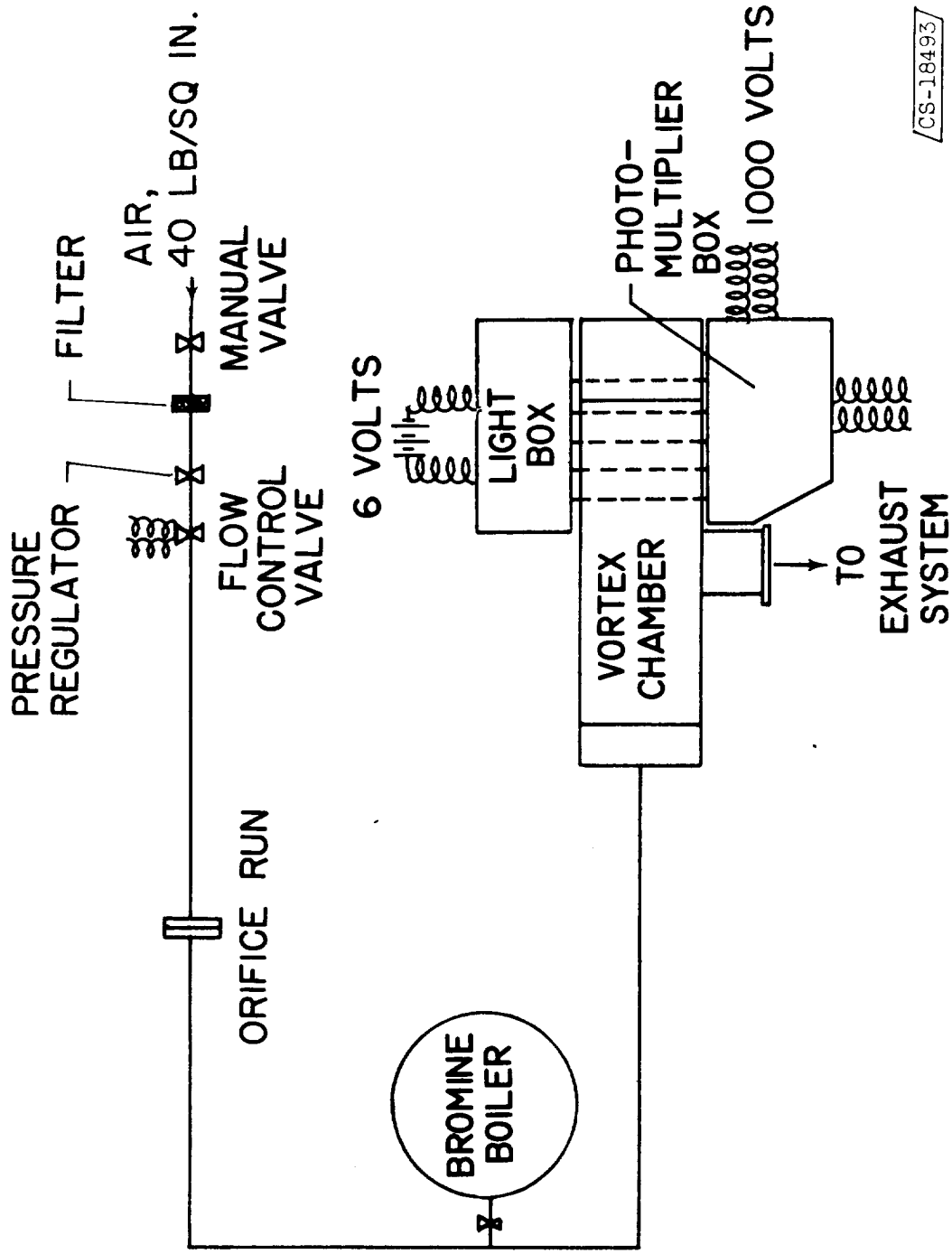

Figure 5. - Schematic drawing of air-bromine vortex system.

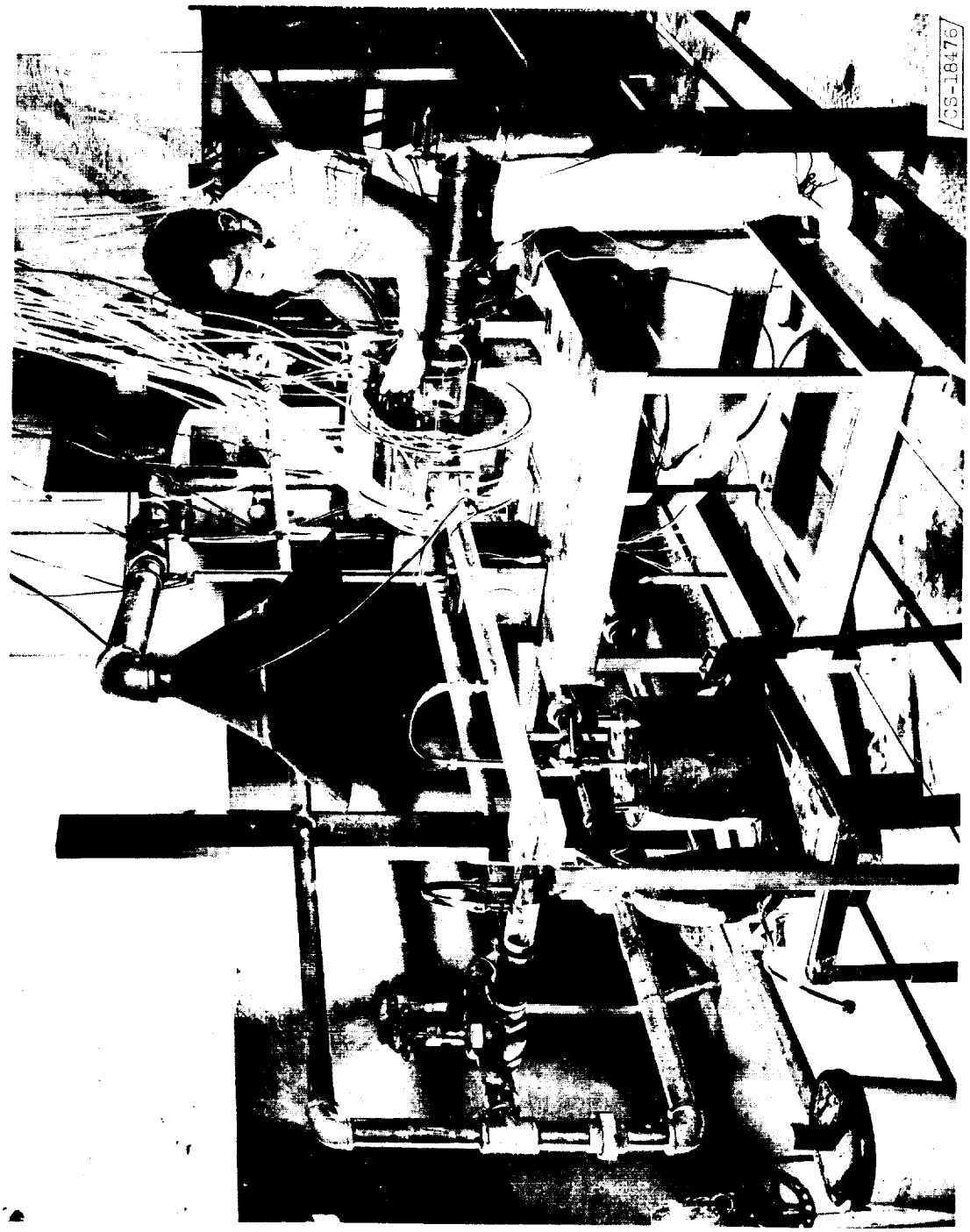

Figure 6. - Overall vortex test setup.

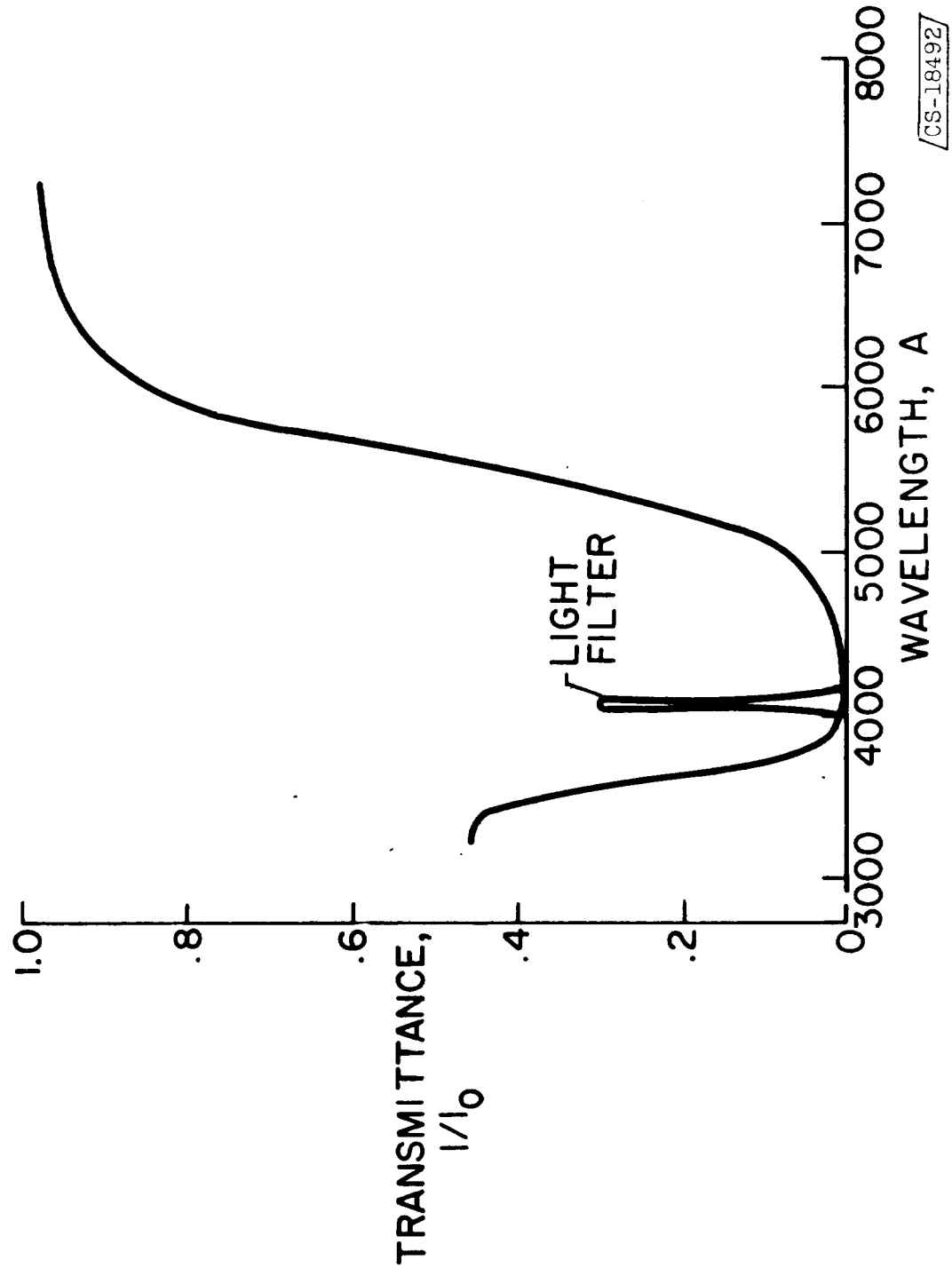

Figure 7. - Light-absorption curve of bromine gas.

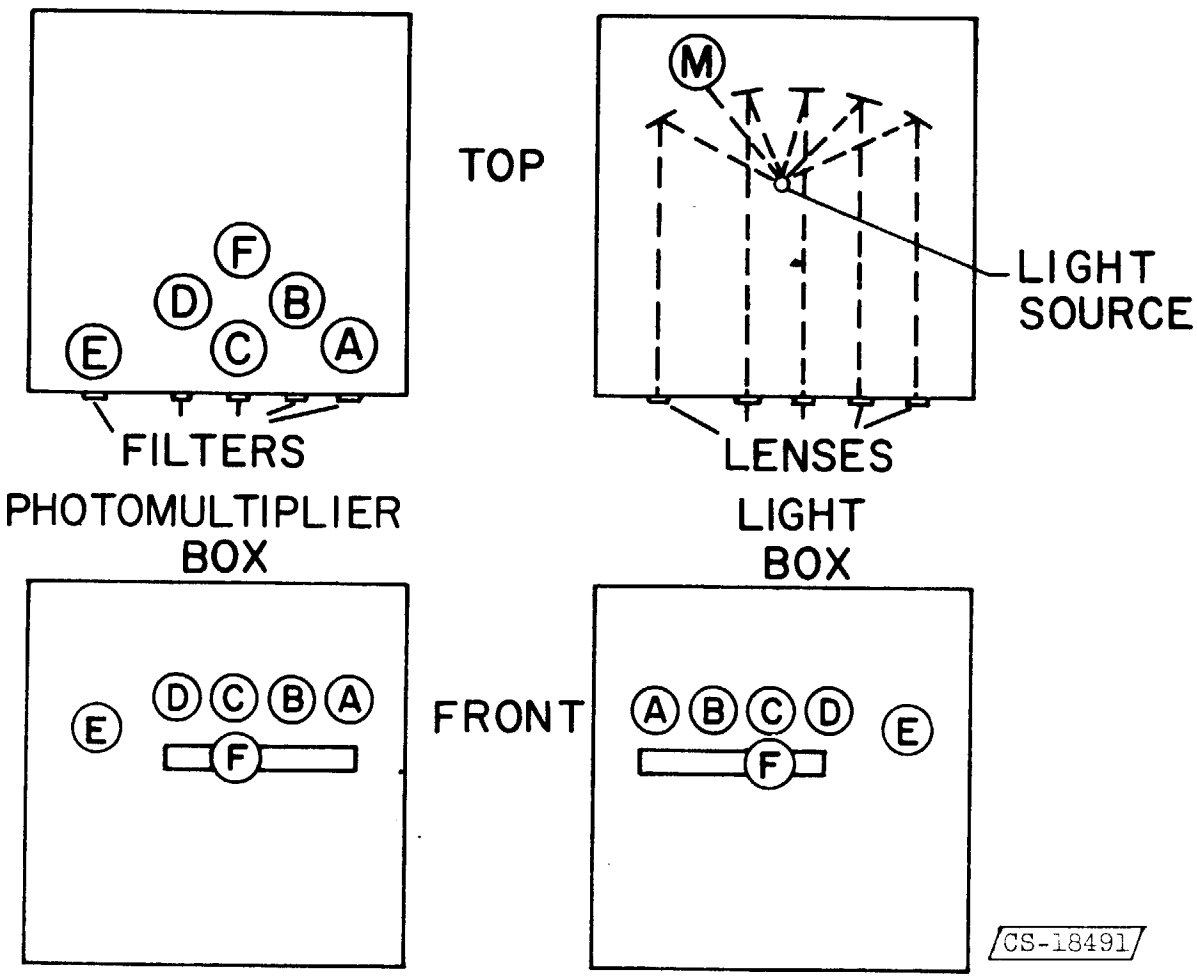

Figure 8. - Schematic drawing of vortex optical instrumentation.

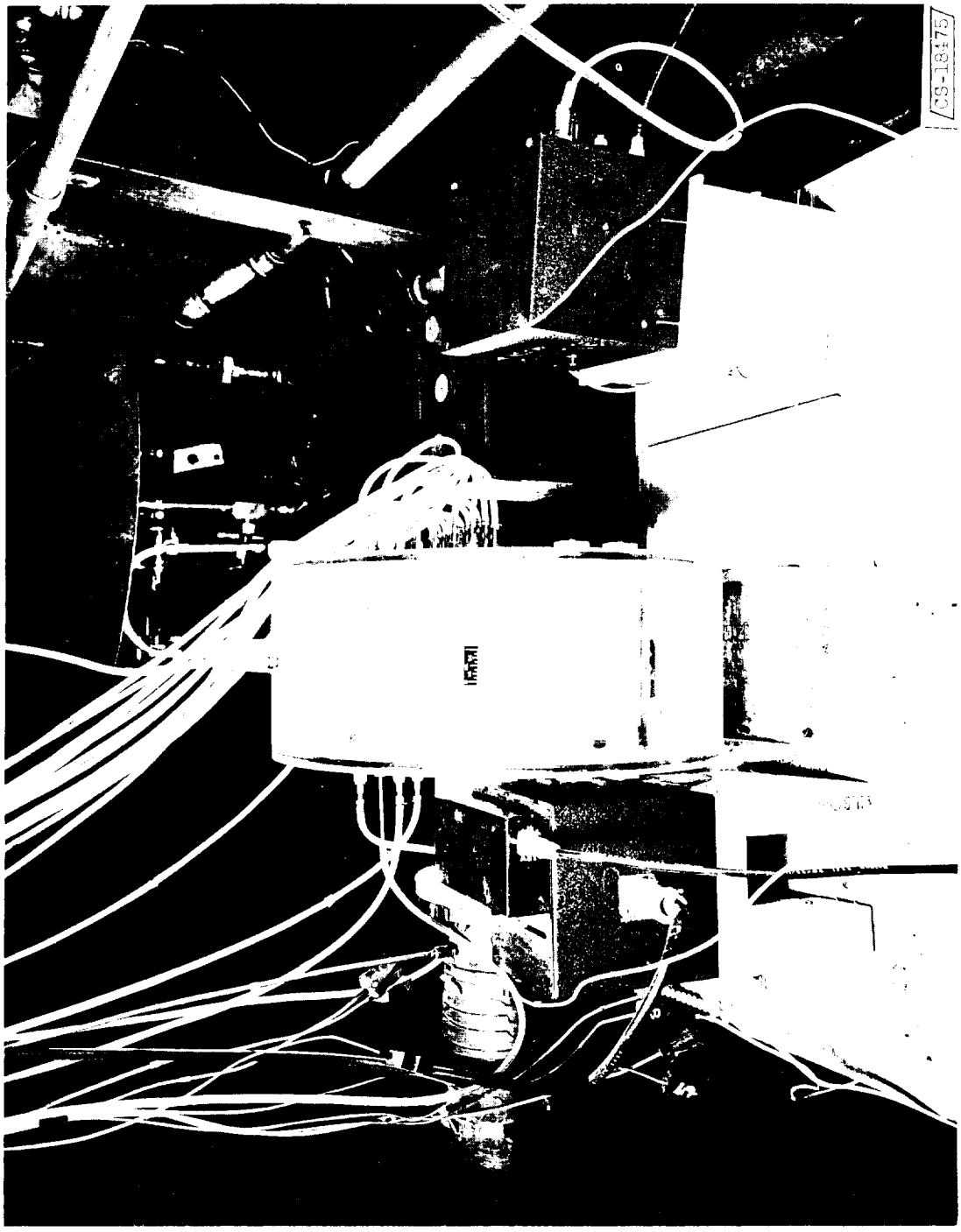

Figure 3. - Layout of vortex optical instrumentation.

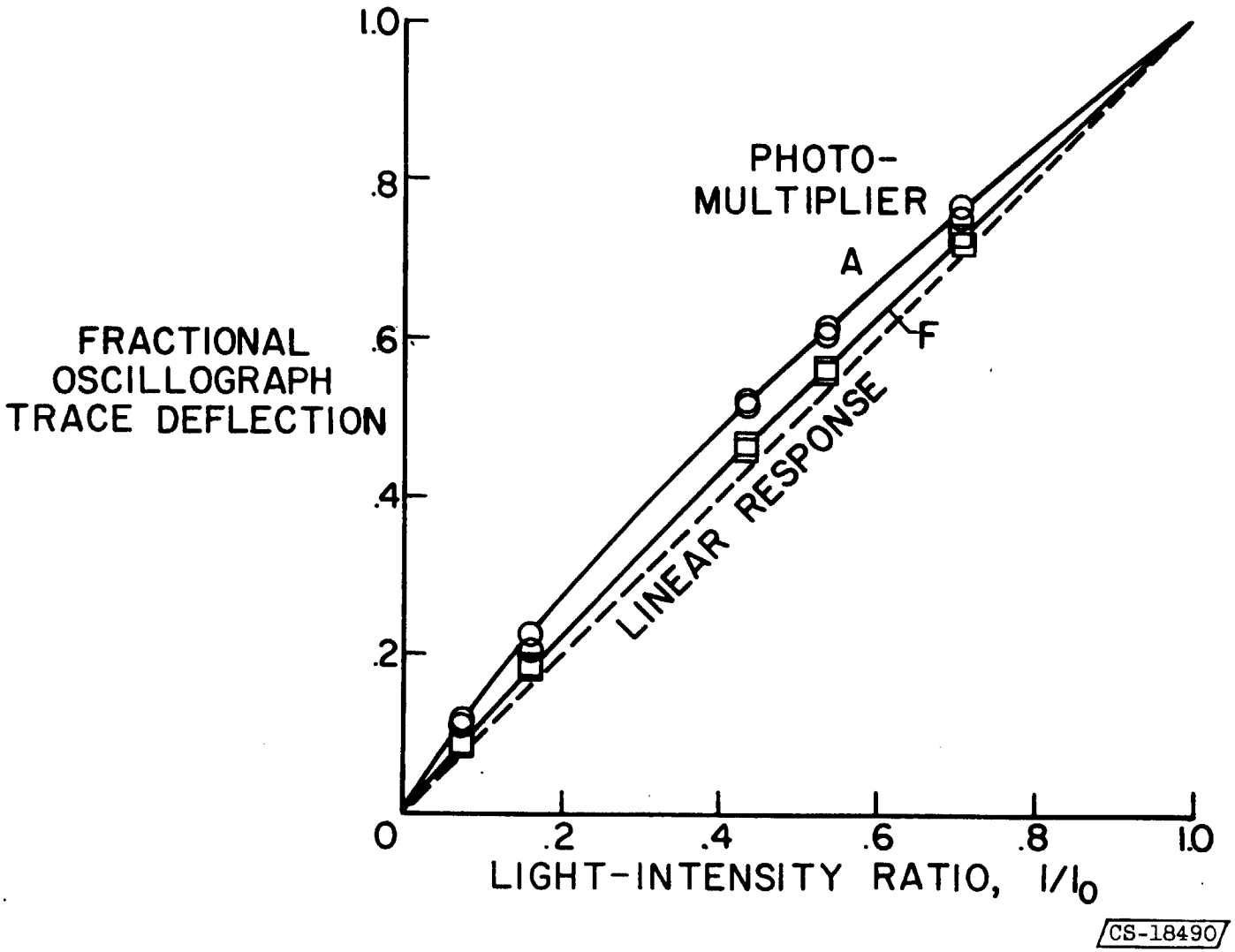

Figure 10. - Typical photomultiplier calibration curves.

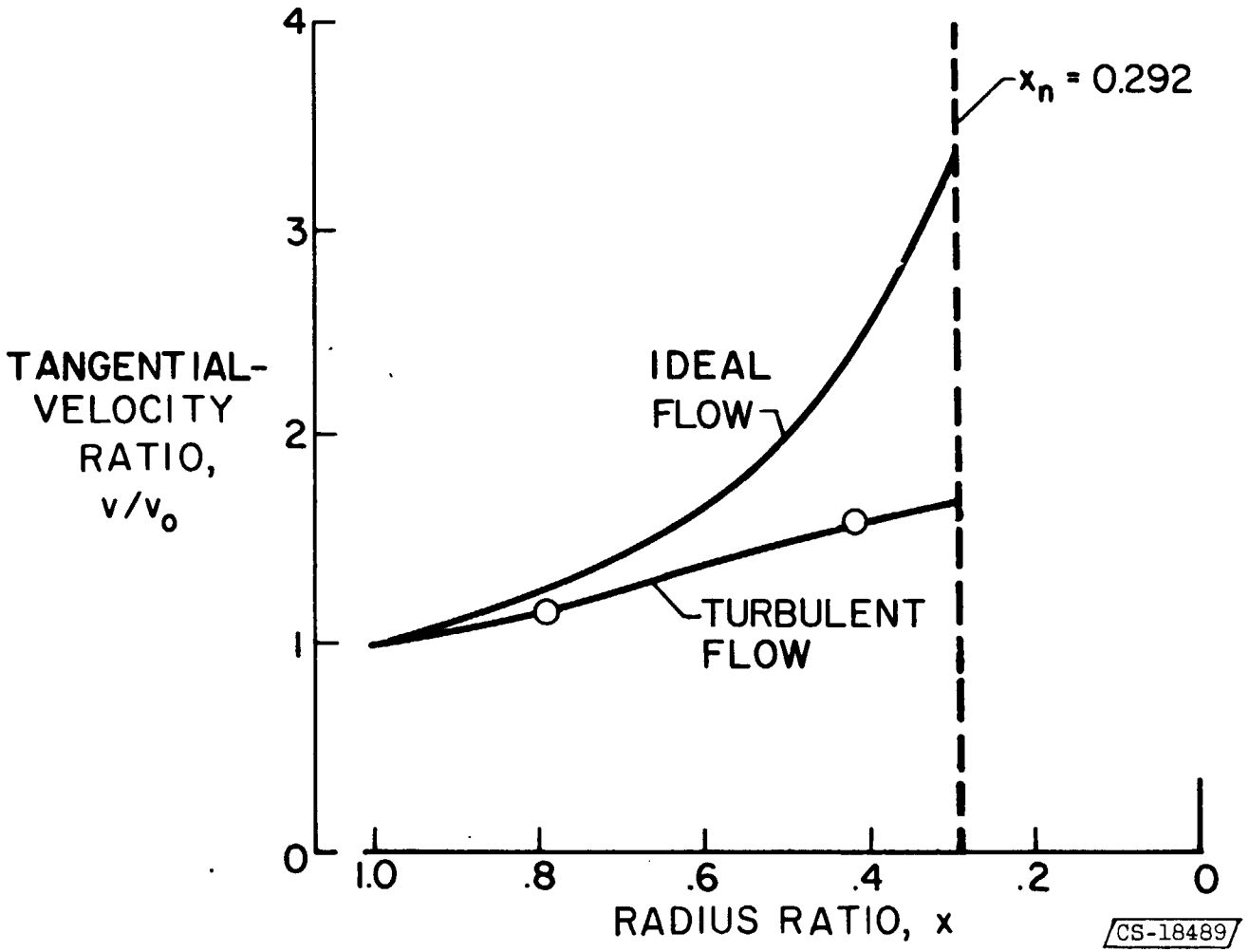

Figure 11. - Velocity-ratio data and analytical curves. Tangential velocity at outer radius, 228 feet per second; Reynolds number, 2.4; airflow rate, 0.1 pound per second.

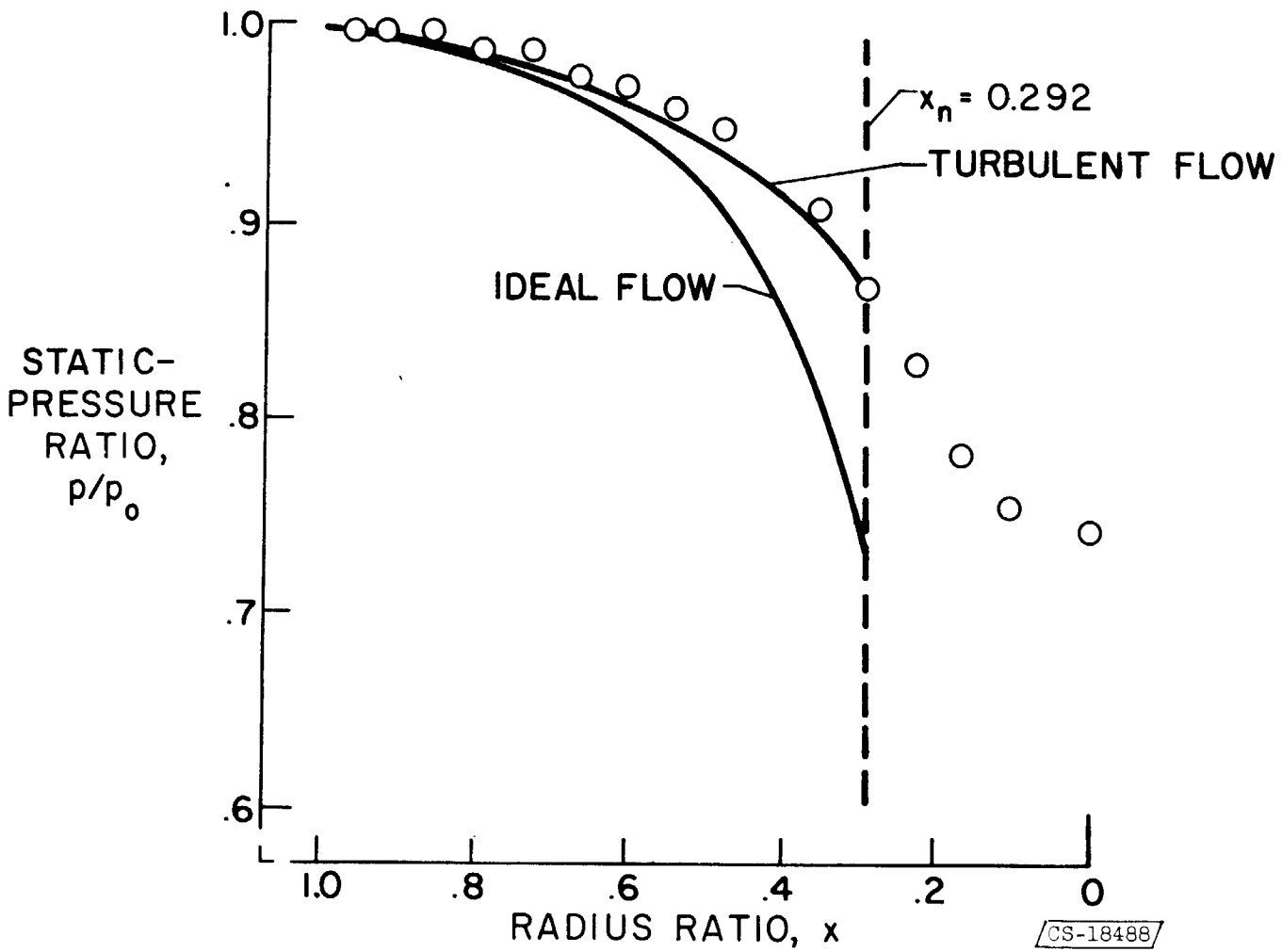

Figure 12. - Static-pressure-ratio data and analytical curves. Tangential velocity at outer radius, 228 feet per second; Reynolds number, 2.4; airflow rate, 0.1 pound per second.

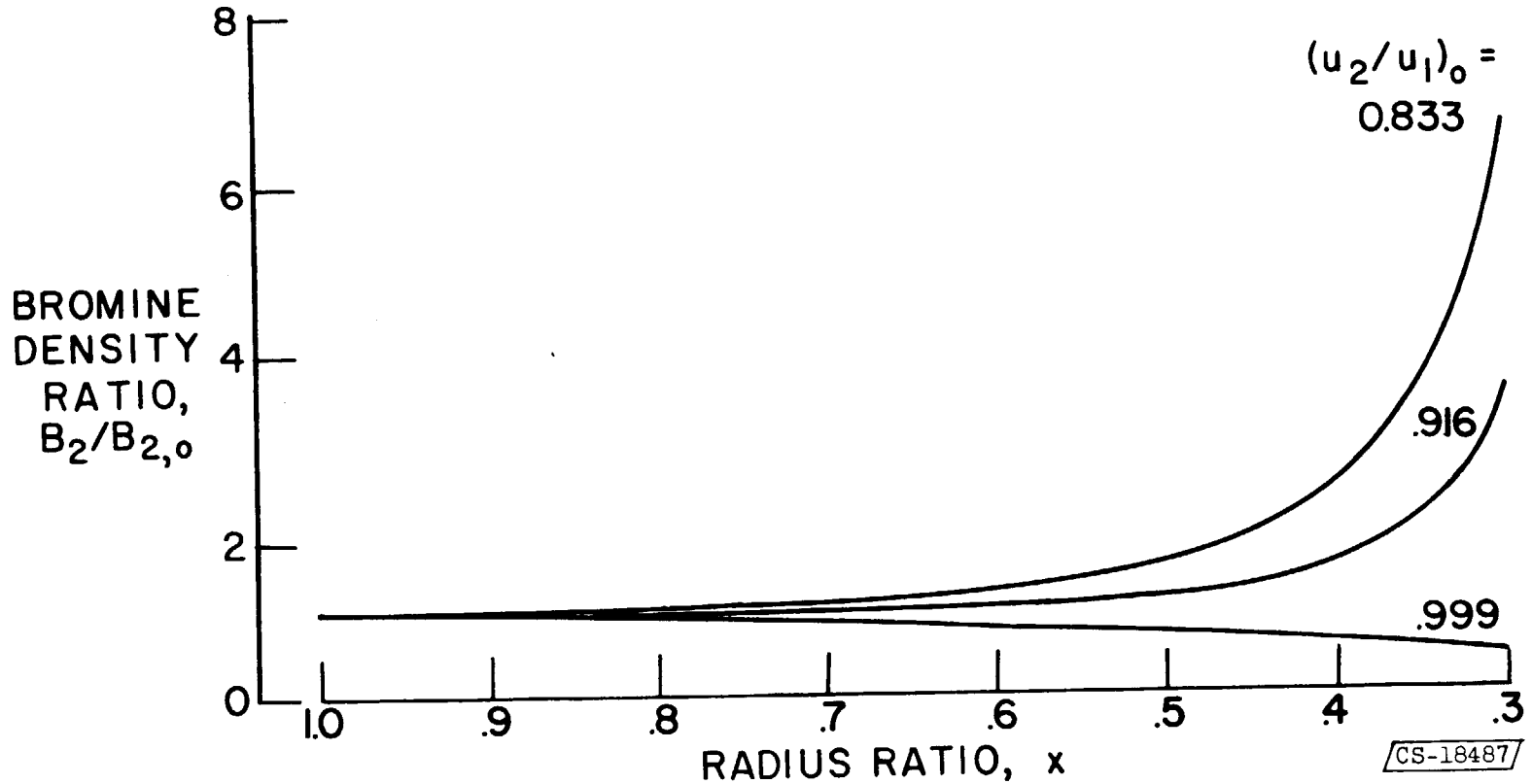

(a) Effect of boundary value $(u_2/u_1)_o$. Tangential velocity at outer radius, 500 feet per second; Reynolds number, 2.6; airflow rate, 0.1 pound per second; weight-flow ratio, 1000.

Figure 13. Analytical density curves for air-bromine mixture.

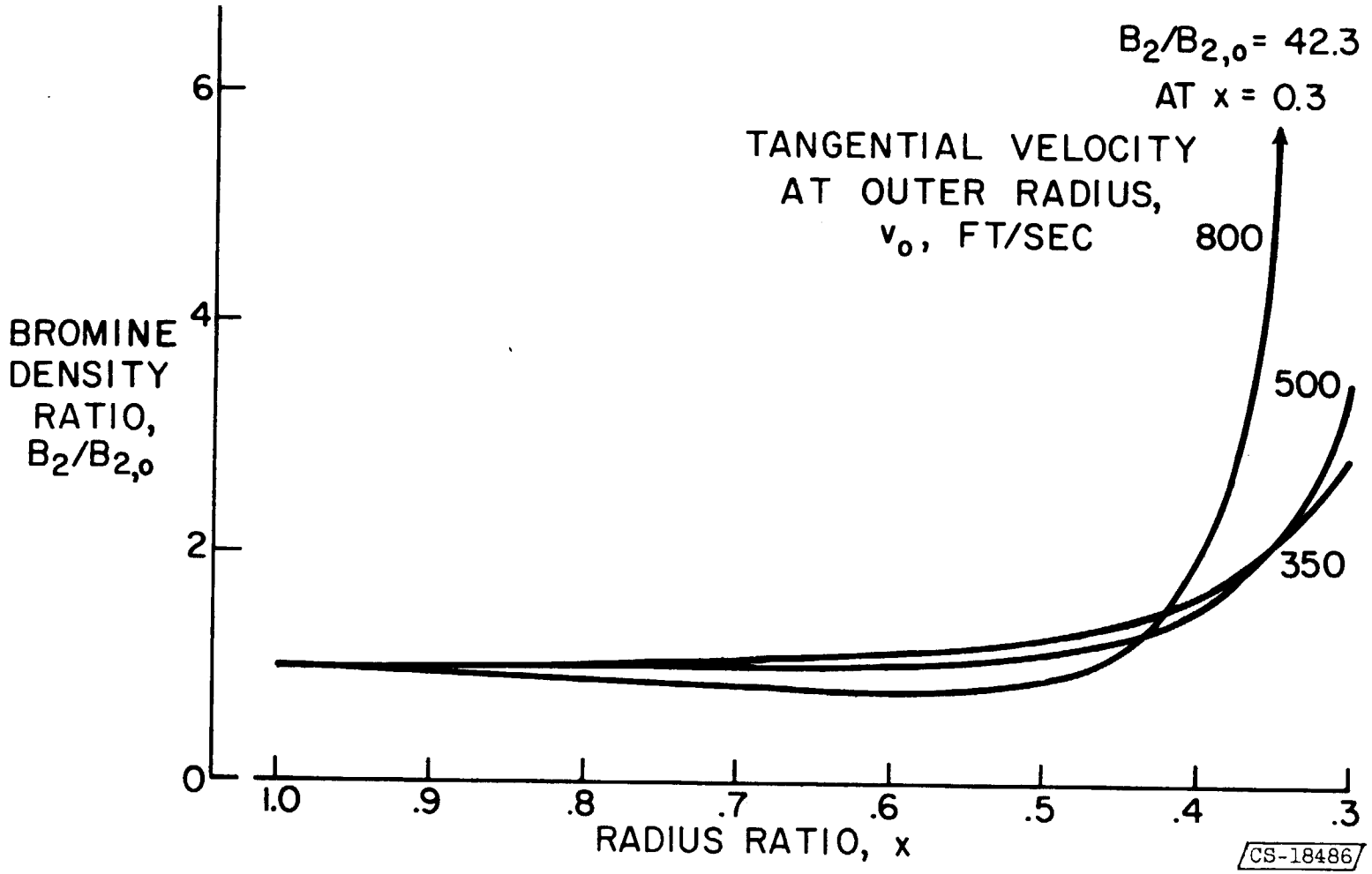

(b) Effect of velocity. Radial-velocity ratio, 0.916; Reynolds number, 2.6; airflow rate, 0.1 pound per second; weight-flow ratio, 1000.

Figure 13. - Continued. Analytical density curves for air-bromine mixture.

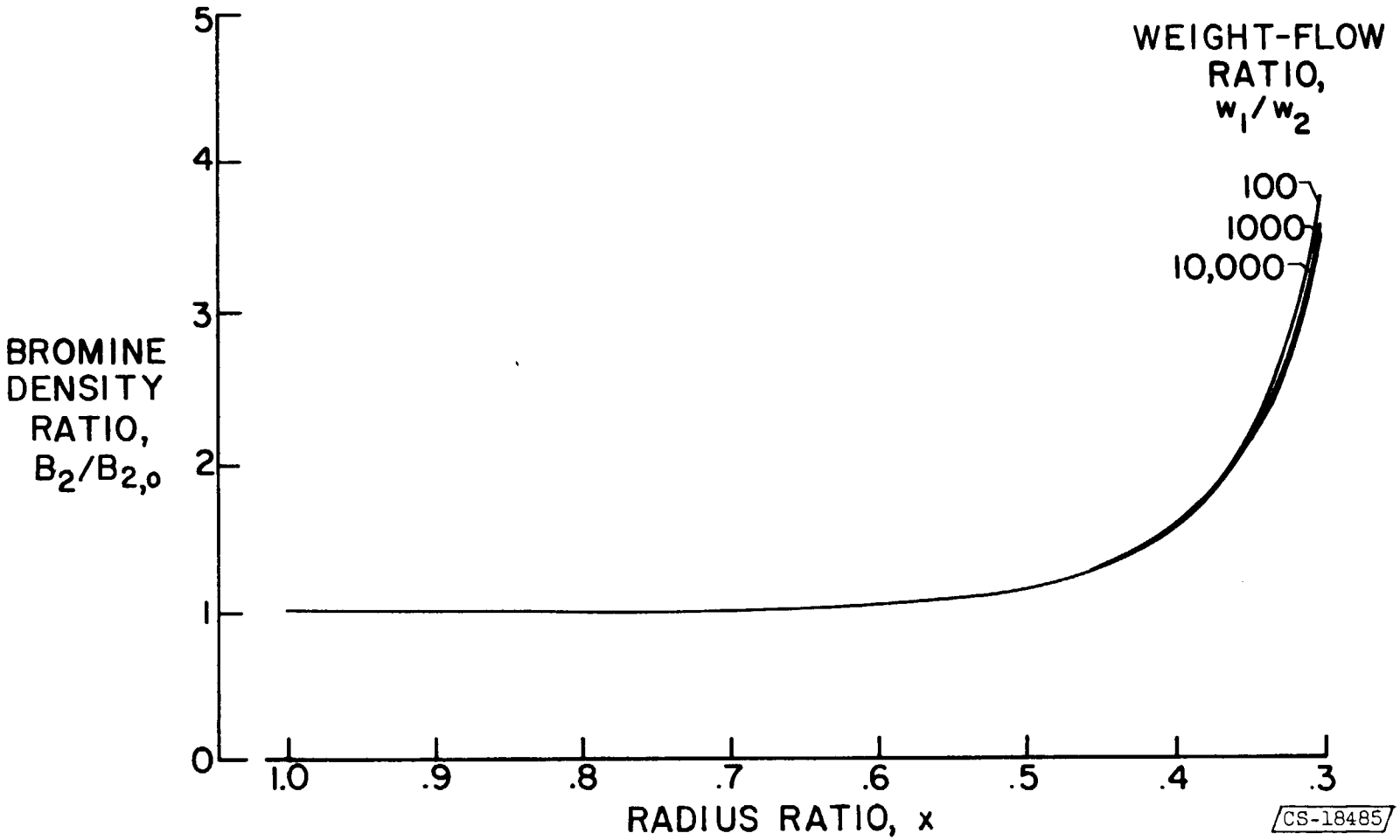

(c) Effect of air-to-bromine weight-flow ratio. Radial-velocity ratio, 0.916; tangential velocity at outer radius, 500 feet per second; Reynolds number, 2.6; airflow rate, 0.1 pound per second.

Figure 13. - Continued. Analytical density curves for air-bromine mixture.

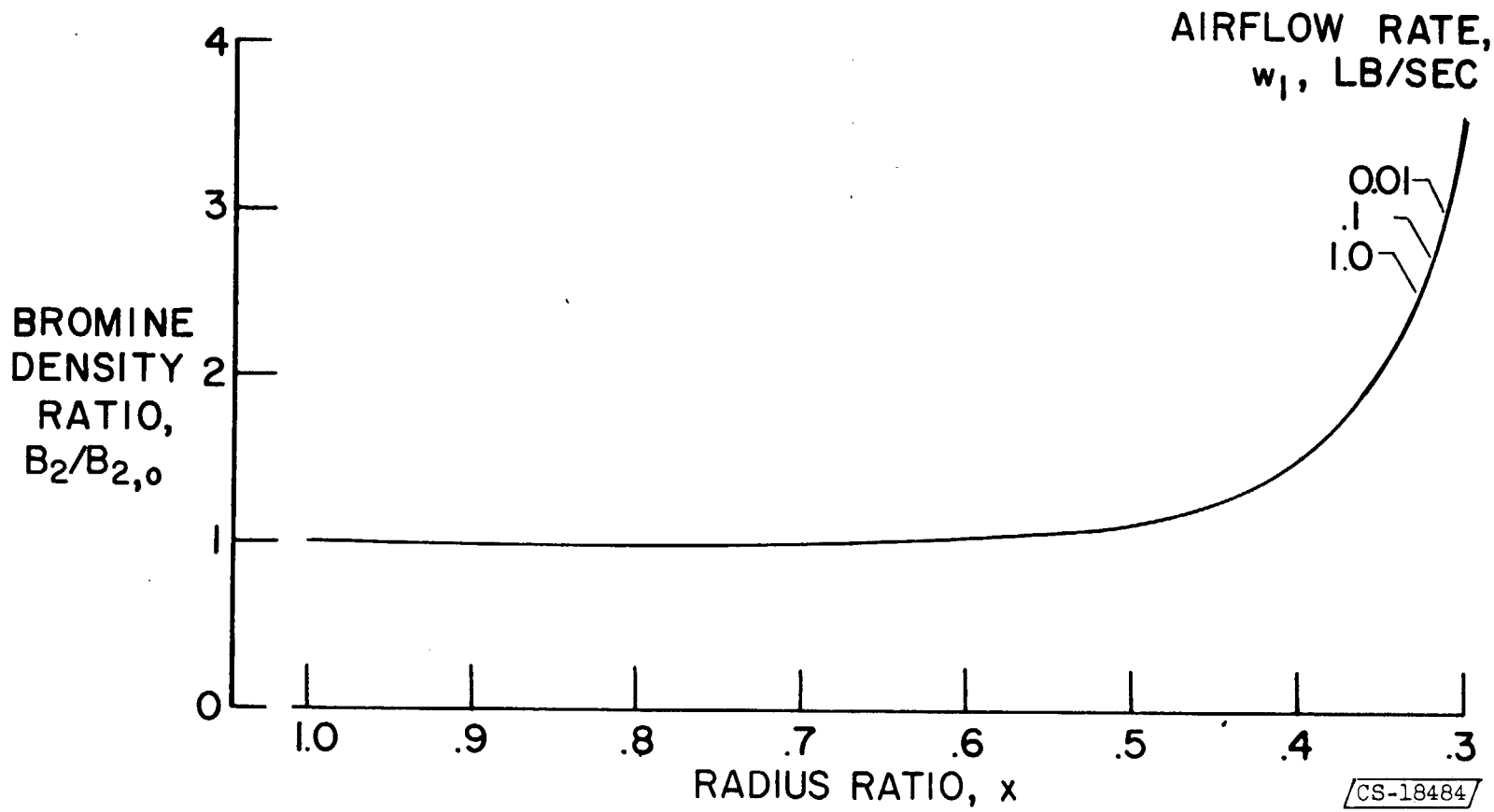

(d) Effect of airflow rate. Radial-velocity ratio, 0.916; tangential velocity at outer radius, 500 feet per second; Reynolds number, 2.6; bromine flow rate, 0.0001 pound per second.

Figure 13. - Continued. Analytical density curves for air-bromine mixture.

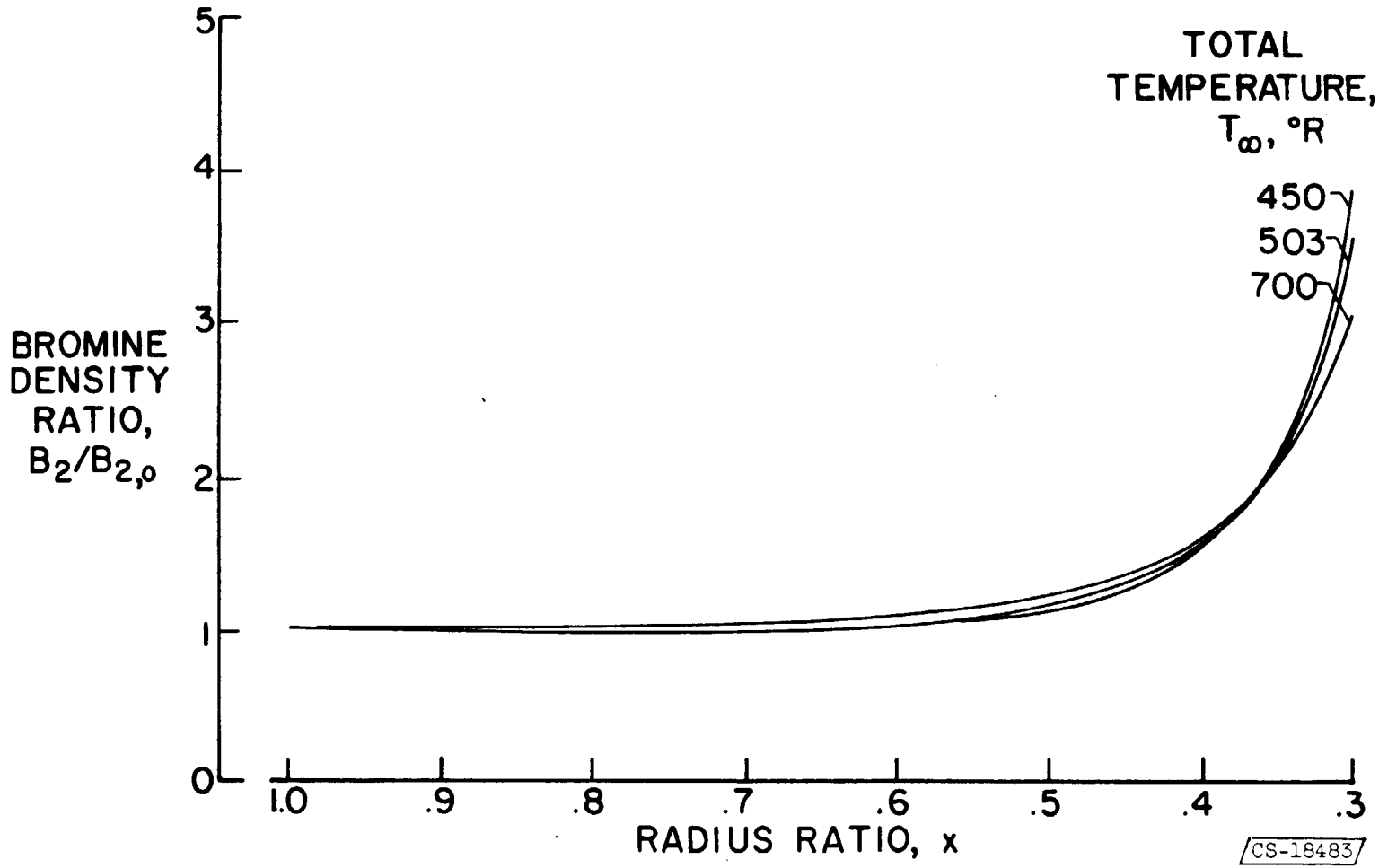

(e) Effect of temperature. Radial-velocity ratio, 0.916; tangential velocity at outer radius, 500 feet per second; Reynolds number, 2.6; airflow rate, 0.1 pound per second; weight-flow ratio, 1000.

Figure 13. - Continued. Analytical density curves for air-bromine mixture.

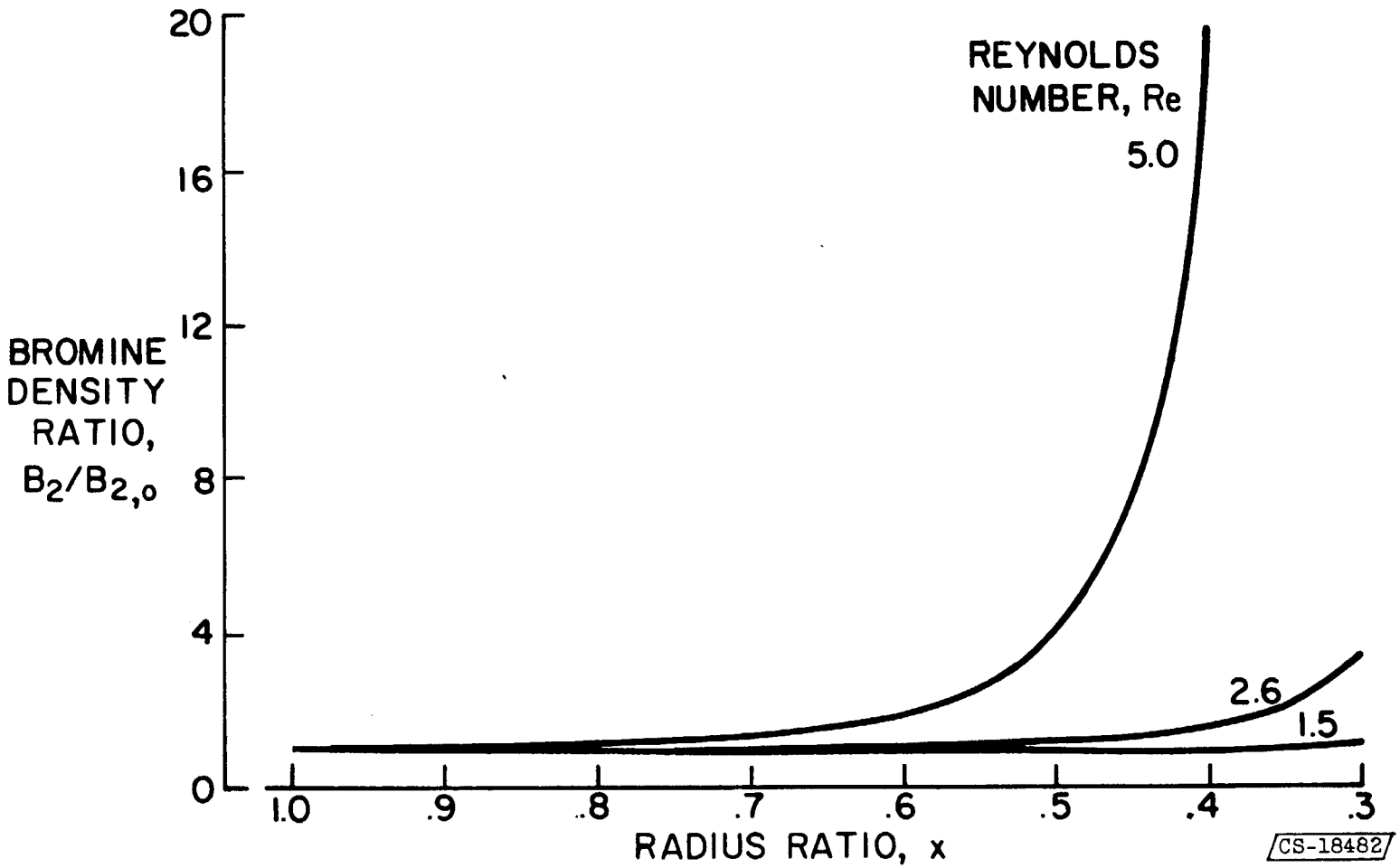

(f) Effect of turbulence. Radial-velocity ratio, 0.916; tangential velocity at outer radius, 500 feet per second; airflow rate, 0.1 pound per second; weight-flow ratio, 1000.

Figure 13. - Concluded. Analytical density curves for air-bromine mixture.

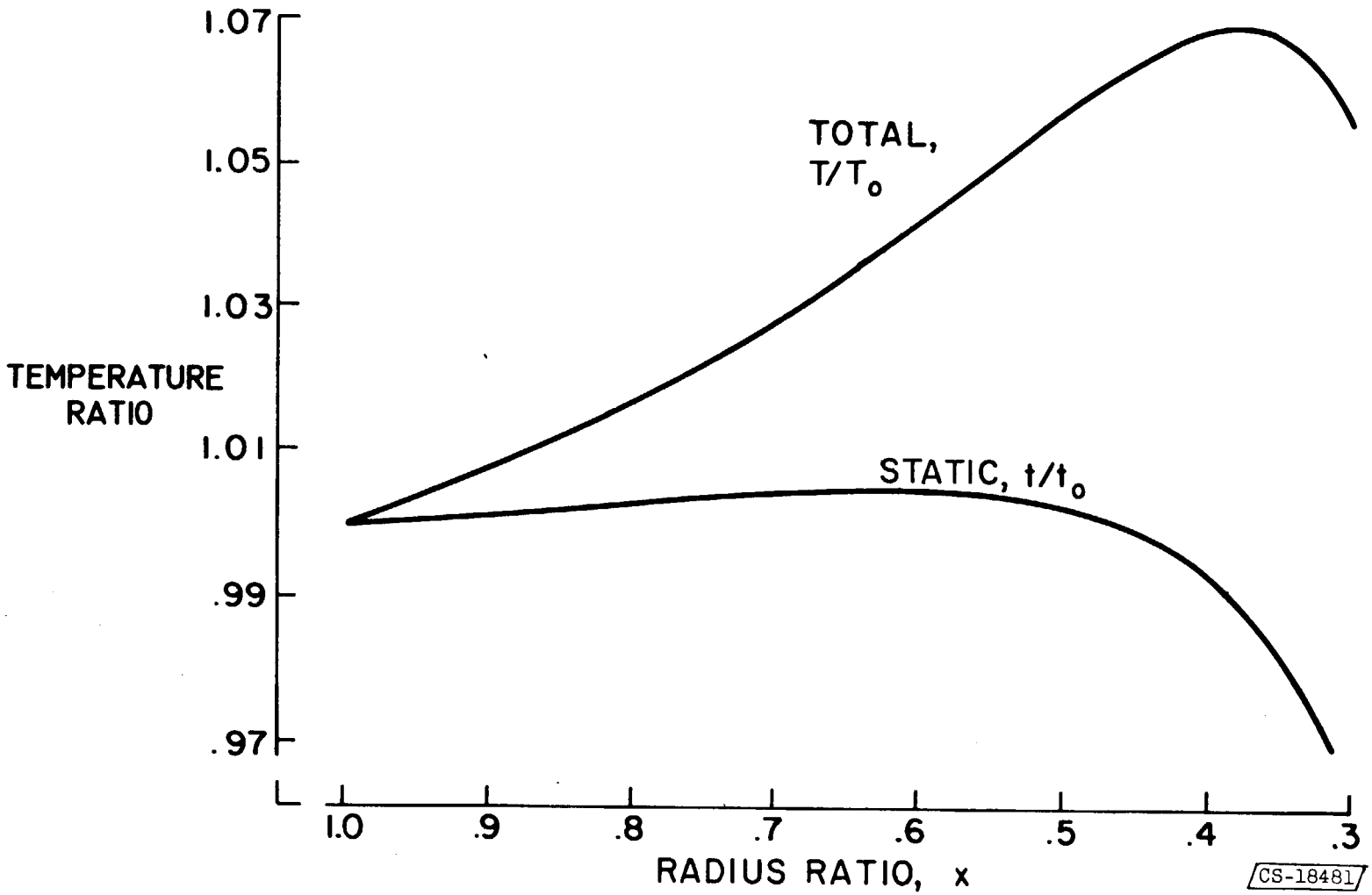

Figure 14. - Analytical temperature ratio for air-bromine mixture. Radial-velocity ratio, 0.916; tangential velocity at outer radius, 500 feet per second; Reynolds number, 2.6; airflow rate, 0.1 pound per second; weight-flow ratio, 1000.

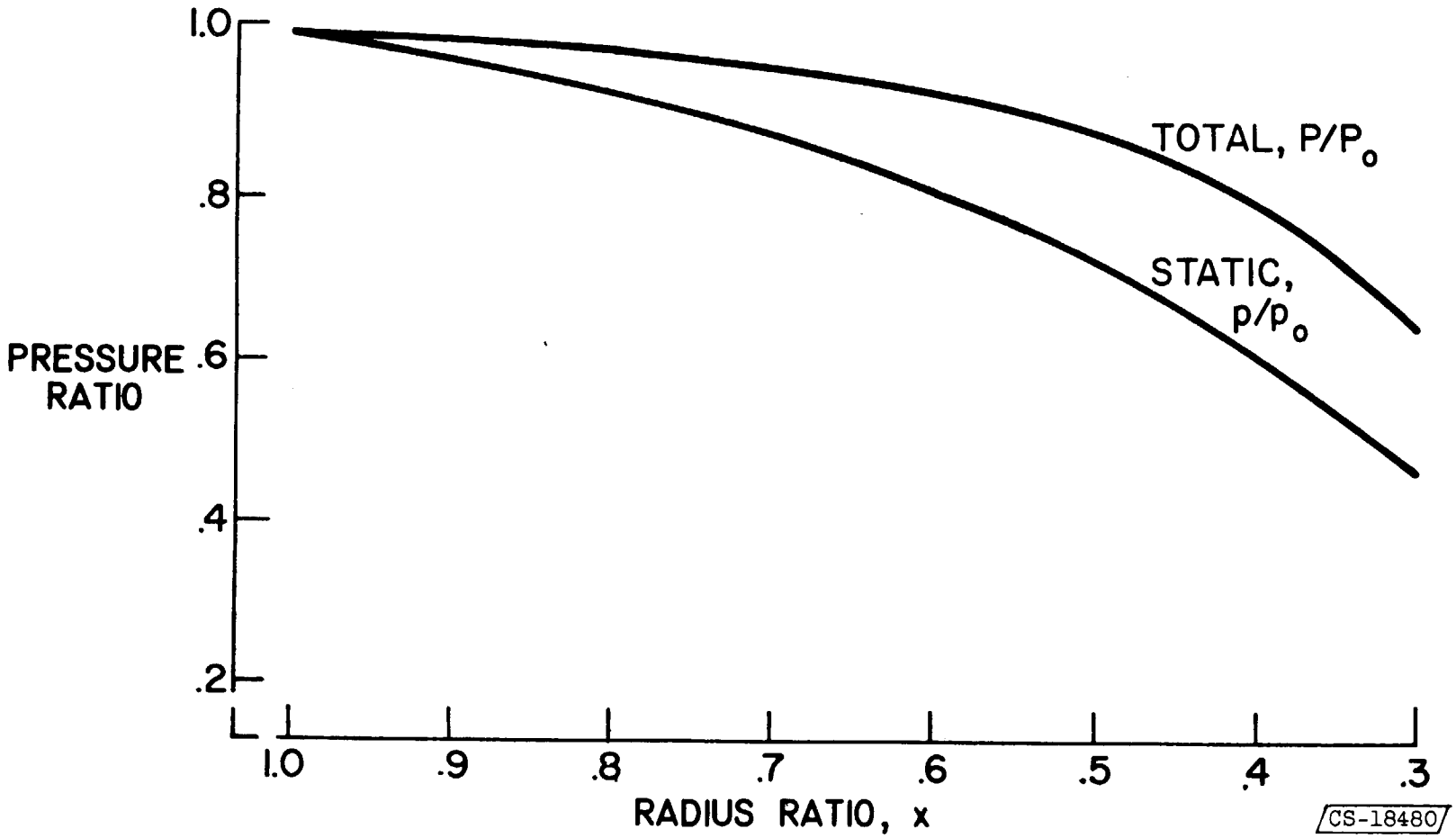

Figure 15. - Analytical pressure ratio for air-bromine mixture. Radial velocity ratio, 0.916; tangential velocity at outer radius, 500 feet per second; Reynolds number, 2.6; airflow rate, 0.1 pound per second; weight-flow ratio, 1000.

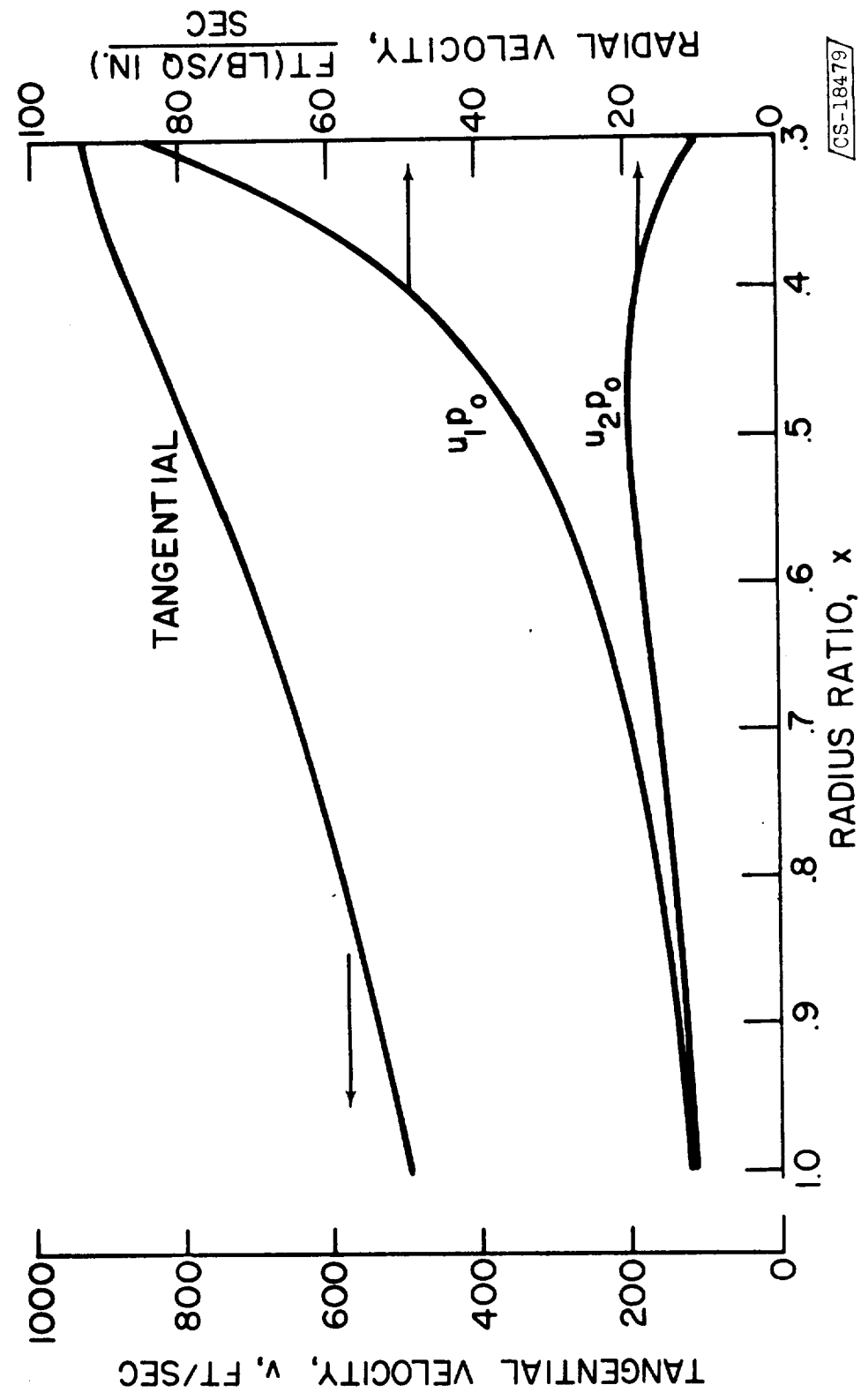

Figure 16. - Analytical velocities for air-bromine mixture. Radial-velocity ratio, 0.916; tangential velocity at outer radius, 500 feet per second; Reynolds number, 2.6; airflow rate, 0.1 pound per second; weight-flow ratio, 1000.

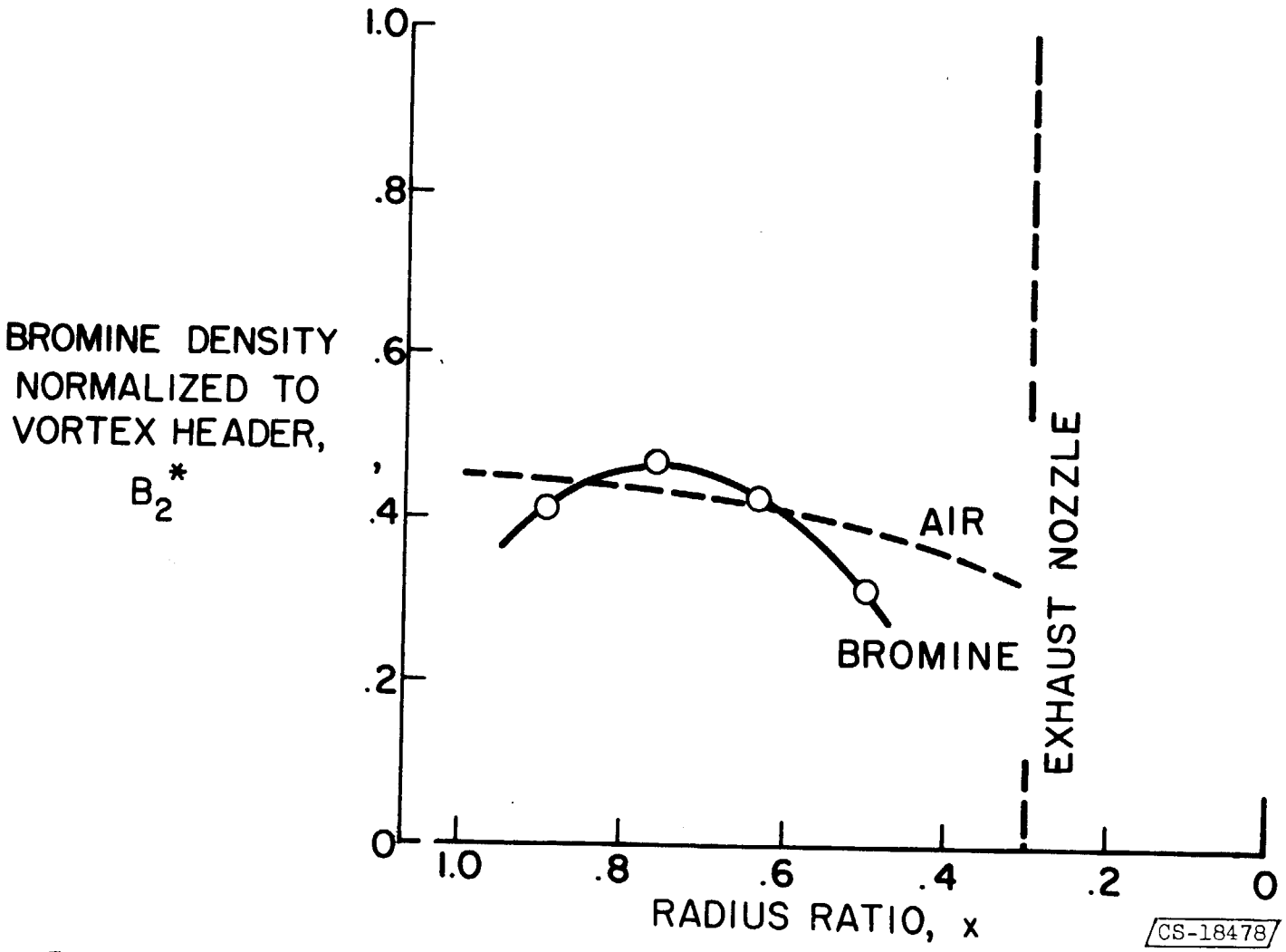

Figure 17. - Experimental bromine density variation. Tangential velocity at outer radius, 477 feet per second; Reynolds number, 2.1; airflow rate, 0.115 pound per second; bromine flow rate, 0.00234 pound per second.

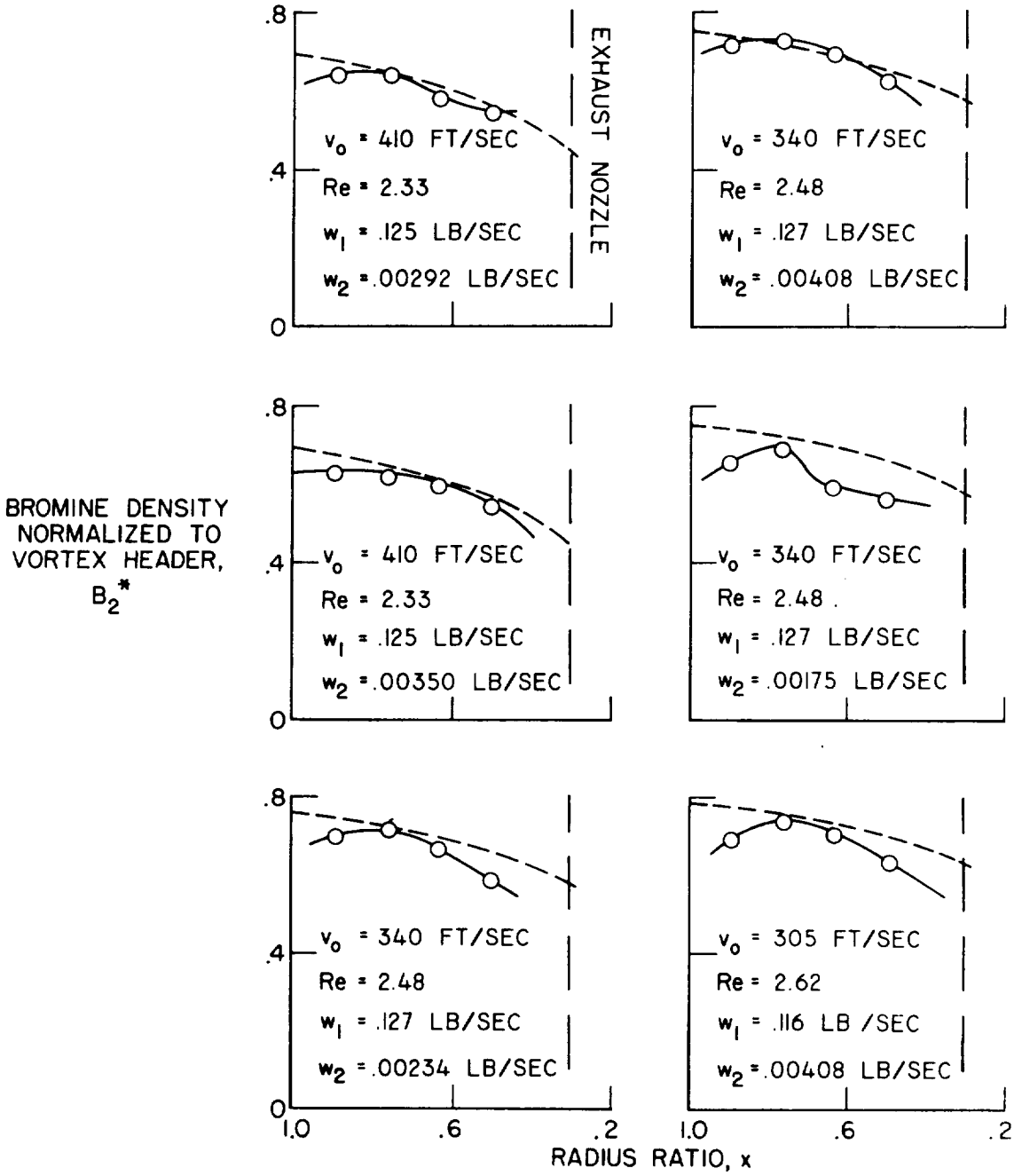

Figure 19. - Typical experimental bromine density [illegible].